Journal of Visualized Experiments

Plasma actuators in rarefied super/hypersonic flows: experimental works to enhance spacecraft control and deceleration during atmospheric entries.

--Manuscript Draft--

Manuscript Number:	JoVE56602R2
Full Title:	Plasma actuators in rarefied super/hypersonic flows: experimental works to enhance spacecraft control and deceleration during atmospheric entries.
Article Type:	Invited Methods Article - JoVE Produced Video
Keywords:	Gas and Plasma Physics; Compressible Aerodynamics; Super/hypersonic flows; Atmospheric entries; Aerospace engineering; Rarefied flows; Wind tunnel; Shock wave; Spacecraft control.
Manuscript Classifications:	90.09: Research and Support Facilities (Air); 91.12: Astronautics (General); 91.14.18: ground support facilities (space); 91.18: Spacecraft Design, Testing and Performance; 93.34: Fluid Mechanics and Thermodynamics; 97.75: Plasma Physics
Corresponding Author:	Sandra Coumar, Ph.D Centre National de la Recherche Scientifique Orléans, Loiret FRANCE
Corresponding Author Secondary Information:	
Corresponding Author E-Mail:	sandra.coumar@cnrs-orleans.fr
Corresponding Author's Institution:	Centre National de la Recherche Scientifique
Corresponding Author's Secondary Institution:	
First Author:	Sandra Coumar, Ph.D
First Author Secondary Information:	
Other Authors:	Viviana Lago
Order of Authors Secondary Information:	
Abstract:	During a reentry mission, the deceleration is a major issue. The main way to slow down the vehicle is to rely on the drag force induced by the friction with the air. However, considering the high speeds reached by the vehicle, the friction induces an intense heat of the structure of the vehicle. To counter this, the authors present a new method based on the ionization of the flow around the vehicle with a plasma actuator leading to the deceleration of the vehicle. The main point of this technique is that it allows the vehicle to be slowed in the highest layers of the atmosphere before it even endures the hard conditions due to the atmospheric friction. The present paper introduces the implementation of the plasma actuator on a beveled flat plate, which is a classic model in aerodynamic studies. The reentry conditions are simulated with the super/hypersonic low-density wind tunnel MARHy located in the ICARE laboratory. Therefore, the method is a several steps process divided in two main parts: the manufacturing of the plasma actuator and the settling of the wind tunnel in order to deliver the chosen flow conditions. The experimental setup is undertaken with a great care as it will suffer high-speed flows, high temperature and also in our case, low pressure. For the aerodynamic study, three types of diagnostics are utilized: an intensified camera for the visualization of the flow, an infra-red camera to follow the evolution in time of the distribution of the surface temperatures and a Pitot probe used for the mapping or the flow pressures around the model. Even though this method is used as the basis for our experiments, it is adapted depending on the flow generated by the wind tunnel, the shape of the plasma actuator or the applied diagnostics.
Author Comments:	We can propose a short movie (2 sec) showing the opening of the shock wave when

	increasing the plasma power.
Additional Information:	
Question	**Response**
If this article needs to be "in-press" by a certain date, please indicate the date below and explain in your cover letter.	09-01-2017

TITLE:

Plasma Actuators in Rarefied Super/Hypersonic Flows: Experimental Work to Enhance Spacecraft Control and Deceleration During Atmospheric Entries

AUTHORS & AFFILIATION:

Sandra Coumar, Viviana Lago

ICARE, CNRS, UPR 3021, Orléans Cedex 2, France

E-MAIL ADDRESSES:

Sandra Coumar (sandra.coumar@cnrs-orleans.fr)
Viviana Lago (vivina.lago@cnrs-orleans.fr)

CORRESPONDING AUTHOR:

Sandra Coumar
Email Address: sandra.coumar@cnrs-orleans.fr
Tel: (+33)-238-257778

KEYWORDS:

Gas and plasma physics, compressible aerodynamics, super/hypersonic flows, atmospheric entries, aerospace engineering, rarefied flows, wind tunnel, shock wave, spacecraft control

SHORT ABSTRACT:

A protocol for the setup of a plasma actuator, designed for atmospheric entries and placed into supersonic rarefied flow generated with a wind tunnel, is presented.

LONG ABSTRACT:

During an atmospheric reentry mission, deceleration is a major issue. The main way to slow down a vehicle is to rely on the drag force induced by the friction with the air. However, due to the high speeds reached by the vehicle, the friction induces intense heating of the structure of the vehicle. To counter this, the authors present a new method based on the ionization of the flow around the vehicle with a plasma actuator leading to the deceleration of the vehicle. The main point of this technique is that it allows the vehicle to be slowed in the highest layers of the atmosphere before it endures the harsh conditions produced by atmospheric friction.

This paper introduces the implementation of the plasma actuator on a beveled flat plate, which is a classic model in aerodynamic studies. The reentry conditions are simulated with the super/hypersonic low-density wind tunnel MARHy (Mach Adaptable Rarefied Hypersonic) located in the ICARE laboratory. The method involves two steps: the manufacturing of the plasma actuator and the settling of the wind tunnel to deliver the chosen flow conditions. The experimental setup is carefully designed for high-speed flows, high temperatures and, in our case, low pressures.

For the study of aerodynamics, three types of diagnostics are utilized: an intensified camera for

the visualization of the flow, an infrared camera to follow the evolution in time of the distribution of the surface temperatures, and a Pitot probe used for the mapping of the flow pressures around the model. This method is used as the basis for our experiments and is adapted according to the flow later generated by the wind tunnel, the shape of the plasma actuator, or the applied diagnostics.

INTRODUCTION:

Every space or ballistic mission consists of three phases: launch, flight, and reentry[1]. A successful mission depends on adequate management of the three phases, yet atmospheric reentry has continued to pose major challenges over the past several decades. The very high speeds reached by the vehicle during reentries induce extreme conditions and at least three reentry tasks should be approached with care: deceleration, heating management, and accuracy of the vehicle localization and velocity when landing. Aerodynamic forces, such as drag and lift, become increasingly important as the altitude decreases and usually become dominant at 40 km. This is due to the exponential increase of the air density as distance to the ground decreases. At such altitudes, the drag force plays a key role over all others, including gravity and lift. It influences deceleration and thereby, the heat loads, vehicle design, and re-entry trajectory. Controlling the drag force is a method of directly influencing the deceleration and, therefore, the re-entry conditions.

Previous work carried out by our team showed that plasma actuators induce an increase in the drag force[2] on the model surface and thus, reduce the local heat flux. This effect is obtained by the modification of the shock wave shape that arises when the plasma actuator is on. Therefore, plasma actuators can be classified as a flow control method and compared to traditional techniques. The key strengths of plasma actuators are their low weight and size and relatively low energy consumption. These assets make them promising for flight control systems at high velocities[3]. Hypersonic missions are of great interest, though most of the technologies for hypersonic flow control are complex, time-, and energy-consuming, whereas plasma actuators could be a smart alternative.

However, although many studies deal with plasma control applied to supersonic flows[4-10], few concern rarefied flows, and still fewer focus on experimental analyses. The most striking project in the field of plasmas for aerodynamic purposes is the Ajax project. This project has the merit of highlighting the possibilities of the use of plasmas to influence aerodynamics, but as this was focused on Aeronautics and not space sciences, attempts focused on drag reduction. In 1968, Cahn *et al.*[11] in the United States also reported experiments conducted on electrostatic-influenced flows. Therefore, work on this subject has been conducted for many years, though mostly working at pressures higher than that in our experimental conditions, as indicated by the use of the Schlieren technique. Since the mid-1990s, publications in the field of plasma control have exploded. Roth[12] shows that the number of “plasma actuator” entries in an online search has been increasing exponentially since 2003. But, the role of the Electro Hydrodynamic (EHD) effect is much less clear in the case of supersonic flow conditions[13,14] and thermal effects are often forward. Other works are available but they are essentially only numerical analyses[15,16]. Therefore, they are complementary to experimental work but cannot be a substitute, especially

for validating a theoretical hypothesis.

The specific aim of our team is to make use of the wind tunnel MARHy located in the ICARE laboratory to simulate super/hypersonic low-pressure flows, representing different altitudes, to study the implementation of plasma actuators designed to influence the drag on a vehicle during reentry. Hence, the present work provides complementary databases and knowledge to other researchers working at higher pressure and thus, a higher Reynolds number. Our work is unique because we focus on high altitude supersonic and hypersonic applications, which means lower pressures than the studies from other teams. Moreover, we try to increase the drag force for easier control of the spacecraft, whereas the typical approach is to try to decrease it and control the boundary layer separation. Thus, we believe that our research is innovative and complementary to that conducted by other authors in the super/hypersonic domain. Moreover, we have experimental facilities, which allow us to carry out experimental research in the rarefied supersonic/hypersonic domain that can simulate altitudes between 60 and 140 km with Mach numbers ranging between 2 and 20. These experimental results can be useful for the numerical analysis community, which simulates the effects of plasma actuators under such conditions and might need experimental results for the validation of theoretical findings.

PROTOCOL:

1. Experimental Planning

1.1. Follow instructions and safety precautions before entering the wind tunnel's hall. Safety training can be required for new users.

1.2. Schedule the experiments in advance and consider the details of the experiments. After selecting the model to be studied, characterize the plasma actuator: its size, shape, and position on the model.

1.3. Think about the goal of the study and the expected results to install and prepare the diagnostic tools.

1.4. Organize the wind tunnel supplies, such as the order of gas bottles, if needed.

2. Preparation of the Research Object

2.1. Manufacturing the plasma actuator

2.1.1. Manufacture a stencil in the shape and dimensions of the active electrode and, if needed, another one for the grounded electrode. In this paper, both electrodes are rectangular but with rounded corners, with a radius of curvature of 6 mm, in order to avoid electrostatic edge effects. The length of each electrode is 50 mm with a width of 35 mm representing a covering of 35% of the model surface (see **Figure 1**).

2.1.2. Cut the electrodes using the stencil in the aluminum adhesive. This adhesive is selected as the electrode material because of its small thickness (a few micrometers), high temperature resistance, and high electrical conductivity, all of which minimize losses.

2.1.3. Gently remove the adhesive paste with acetone without creasing the electrode.

2.2. Preparation of the flat plate

2.2.1. Design the model taking into account the size of the flow core. In this study, the model is a beveled flat plate of 100 mm-length, 50 mm-width, 4 mm-thickness and 15° leading edge angle. Choose an electrically insulating and heat-resistant material, because ionizing the gas can deform the model. Here, the model is made of quartz (see **Figure 1**).

2.2.2. Drill a hole of 2 mm diameter at 0.7 mm from the left side of the flat plate and 12 mm from its leading edge. For this purpose, use a diamond hollow drill of 2 mm diameter. The hole (Hole 1) is used as a passage for the screw that will hold the high-voltage cable and the model together (see **Figure 2**). The position of the hole is estimated to be minimally cumbersome and placed on the surface of the active electrode.

2.2.3. Drill another hole of 2 mm diameter at 0.7 mm from the left side of the flat plate, but this time 70 mm from the leading edge. This hole (Hole 2) is the passage for the screw that will maintain the grounded cable and the model together (see **Figure 2**).

2.2.4. Scrape the surface on which the plasma actuator is to be placed with 240 grade sandpaper. This will help create roughness and improve the electrode laying.

2.2.5. With great care, clean the model with a 60% rubbing alcohol and make sure there are no particles left on the surface.

2.3. Implementation of the plasma actuator on the model.

2.3.1. Spread a thin even layer of RTV (Room Temperature Vulcanizing) glue with a brush on the back of the electrodes and remove the excess glue to avoid adding thickness between the plate and the electrode. The chosen glue should endure high-temperatures, going to at least 600 °C. Moreover, choose glue with a dilatation coefficient between those of quartz and aluminum to reduce tension.

2.3.2. Place the active electrode close to the leading edge and press it firmly to expel air bubbles. Indeed, if air bubbles remain, they will inflate when the static pressure decreases and this will lead to detachment of the electrode.

2.3.3. Follow the same procedure as in 2.3.1 and 2.3.2 for the grounded electrode and apply it at a distance of 2.5 cm from the active electrode.

2.3.4. Flip the flat plate over and add something heavy on top of it. This will flatten the electrodes against the flat plate.

2.3.5. Let the whole setup dry for 24 h; the glue should be totally dry. Follow the instructions of the glue; some require heating in an oven.

2.3.6. Use black paint which can withstand high temperatures to draw a line along the central axis of the flat plate and two perpendicular lines passing through the center of each electrode (see **Figure 3**). These lines ensure a good emissivity for the infra-red thermography as the emissivity of the electrodes is low ($\varepsilon < 0.1$ for bare aluminum foil).

3. Installation of the Setup in the Wind Tunnel

3.1. Installation of the setup on the standing pole

3.1.1. Set the standing pole in the test chamber of the wind tunnel, taking into consideration the distance over which the flow would remain uniform (see **Figure 4** and **Figure 5**).

3.1.2. Fix the model on the standing pole. It is essential that the whole setup is electrically insulated to avoid electrical interaction with the discharge.

3.1.3. Set the appropriate angle of attack, defined as the angle between the flow axis and the model reference length (longitudinal model axis), with an angle gauge. Here, the angle of attack is 0°. Therefore, the trailing edge of the model would always coincide with the flow axis. Check that the model remains in the core of the flow (see **Figure 6**).

3.1.4. Set a 1 mm wire-diameter K-type thermocouple to get the static temperature. Place it in the test chamber opposite the model, at least 30 cm from the model in order to avoid interactions with the flow.

3.2. Wiring of the plasma actuator

3.2.1. Screw the high-voltage cable to the active electrode through Hole 1.

3.2.2. Put some insulating glue on the top and end of the screw to avoid arcing when firing the electrode.

3.2.3. Tape the cable to the standing pole with Kapton adhesive to prevent it from moving and disturbing the flow. If necessary, insulate exposed conductive material with the Kapton adhesive.

3.2.4. Connect the generator to the high-voltage cable through the vacuum-tight connection. The generator should deliver -10 kV and 100 mA.

3.2.5. Repeat steps 3.2.1 to 3.2.3 with the ground cable but fix it through Hole 2.

3.2.6. With a multimeter, check the electrical insulation between the cathode and the anode and between the cathode and the test chamber.

4. Setting the Diagnostic Tools

4.1. Installation of the Pitot probe

4.1.1. Manufacture the Pitot probe, keeping in mind that it must not interact with the discharge (so, preferably use glass as the material), with a diameter small enough to avoid flow obstruction but not too small to allow reasonable acquisition times[17,18,19].

4.1.2. Place the Pitot tube in the arm of the 3-axis displacement robot (RTA system). The robot is managed via a motion controller, in this case the National Instruments PXI-7344 (see **Figure 7**).

4.1.3. Connect the Pitot tube to the manometer via a plastic tube and seal the connection with a heat shrink.

4.1.4. Set a bypass for the Pitot tube exit to empty the Pitot tube before each new measurement during the test. This will help to initialize the results.

4.1.5. Position the Pitot on the leading edge of the flat plate with the displacement robot. This sets the starting coordinates (X=0 cm, Y=0 cm, Z=0 cm).

4.1.6. Initialize the LabVIEW program meant for data acquisitions for this new test session.

4.2. Installation of the iCCD (Intensified Charge-Coupled Device) camera

4.2.1. Position the camera on the holder and target the setup through the fluorine window (see **Figure 8**). The camera must capture the full side view of the whole flat plate and especially the upper part of the model. Check that the iCCD camera is aligned horizontally with the flat plate axis.

4.2.2. Improve the sharpness of the image communicated by the camera by focusing on one edge of the flat plate.

4.2.3. Take a set of images of the flat plate. They will help for further data comparisons as they show the experimental setup with no disturbances.

4.3. Installation of the IR (Infra-Red) camera

4.3.1. Position the camera on the holder and target the setup through the zinc selenide window (see **Figure 8**). The camera must center the whole flat plate.

4.3.2. Improve the sharpness of the image communicated by the camera by focusing on the upper surface of the flat plate where lines were painted in black, as defined in 2.3.6.

4.3.3. Measure the surface temperature simultaneously with both the IR camera and a K-type thermocouple flush mounted on the flat plate surface. The temperature measured by the IR camera may differ from the one measured by the thermocouple, as the initial calibration of the camera sets the emissivity ε at 1. If so, estimate the real emissivity of the black paint as the ratio of the temperature given by the thermocouple to the temperature given by the IR camera.

4.3.4. Apply the real emissivity to the IR camera calibration to obtain the real surface temperatures with this device.

4.3.5. Set an adequate camera sensitivity range according to the expected results during the test.

5. Running the Facility

5.1. Check the toric joint of the door of the test chamber before closing it and tighten at least one of the two wing nuts to press the door.

5.2. Close all the openings of the wind tunnel.

5.3. Check that the oil of the vane pumps is above the minimum level. If not, fill the reservoir.

5.4. Choose the pumping mode according to the needed static (8 Pa) and stagnation (1,214 Pa) pressures. Some pumping configurations are scheduled in two steps. If this is the case, set a first pump configuration and then the final one when the butterfly valve is opened.

5.5. Do not forget to verify the oil levels and the proper operation of the water pumps during the whole run.

5.6. Once the selected pumping configuration is started, adjust the stagnation pressure with the gas inlet and the static pressure in the test chamber with the butterfly valve.

6. Image of the Baseline

6.1. Do this step before undertaking the experiments. The baseline corresponds to the flat plate in the rarefied flow without firing the discharge. From this, one can calculate the baseline shock wave angle, which is the angle naturally formed between the shock wave and the flat plate because of the supersonic speed of the flow.

6.2. Use the luminescent technique to visualize the airflow and the shock wave (see **Figure 9**).

6.3. The luminescent technique

6.3.1. Install a plate, made from copper or any other conductive material, of dimensions 20 cm x 40 cm above the exit of the nozzle and connect it to the DC power supply.

6.3.2. Install another copper plate of the same dimensions under the exit of the nozzle. This one is grounded. The copper plates must not interfere with the flow.

6.3.3. When the facility is running and delivers the scheduled flow, supply the connected copper plate with -100 V. This will lead to a weak ionization of the flow and allows the visualization of the shock wave but will not influence it.

6.3.4. Utilize each of the diagnostic tools to get baseline results that will serve as comparators for the test results.

7. Firing the Discharge

7.1. Switch on the high-voltage power supply and gradually increase the voltage until the emergence of the glow discharge above the active electrode. Take note of this voltage, which is the breakdown voltage. Here, the breakdown voltage was -0.40 kV.

7.2. Decrease the voltage by -250 V steps and take a set of 250 iCCD images at each voltage. Adjust the exposure time and the gain to get the highest contrast picture but make sure to not saturate the image.

7.3. Take note of the current delivered when biasing the active electrode with the high voltage.

7.4. Simultaneously acquire the temperature distributions on the surface with the IR camera.

7.5. Carry out Pitot profiles for different positions of the Pitot probe for different voltages under the same conditions to get a trend. A standard procedure to establish a complete mapping of the pressure is given below.

7.5.1. Establish a vertical profile at X=0 cm, Y=0 cm, Z=0 cm by increasing the Z-position of the Pitot probe. Register the pressure value after stabilization for each mm in the boundary layer, each 5 mm in the shock wave, and each cm when exiting the flow core.

7.5.2. Move the Pitot probe to X=17.5 cm, which corresponds to the middle of the active electrode and repeat step 7.5.1.

7.5.3. Move the Pitot probe to X=50 cm, which corresponds to the middle of the flat plate, and repeat step 7.5.1.

7.5.4. Move the Pitot probe to X=0 cm and Z=20 cm to perform a longitudinal profile (in the X-

position, the length of the model) and move the Pitot probe by 5 mm.

7.5.5. Repeat step 7.5.4 at position X=0 cm and Z=40 cm.

8. Post-Treating the Results

8.1. iCCD imaging

8.1.1. Process the iCCD set of images with software such as Matlab or ImageJ. For all the discharge conditions, add the 250 images to increase the intensity.

8.1.2. Improve the contrast and make the shock wave angle as visible as possible.

8.1.3. Measure the shock wave angles for each discharge voltage and draw the trend line.

8.1.4. Take measurements of the shock wave stand-off distance from the leading edge.

8.2. Infra-red tomography

8.2.1. Plot the temperature distributions along the black lines for each discharge voltage.

8.2.2. Find the maximum surface temperature and plot it versus the discharge voltage.

8.3. Pitot pressure measurements

8.3.1. As the experimental conditions correspond to the rarefied regime, do any necessary orifice corrections according to the flow conditions and the Pitot reference dimensions as specified by Potter *et al.*[17,18,19].

8.3.2. Draw all the Pitot profiles on the same graph to aid in further comparison.

Note: It can be useful to simulate the experimental case with a numerical code (in this paper, a Monte-Carlo probabilistic code is used) to calibrate the experimental Pitot profiles.

REPRESENTATIVE RESULTS:

The experiments are carried out in the wind tunnel MARHy at the ICARE laboratory located in Orléans (CNRS, National Scientific Research Center, France). MARHy is a low-density facility used for both academic and industrial research. The wind tunnel was built in 1963 at the "Laboratoire d'Aérothermique" and was known as the "SR3" wind tunnel[20] until its relocation in 2000 at the CNRS Orléans. The MARHy wind tunnel can be equipped with a wide range of nozzles allowing the generation of subsonic, supersonic, and hypersonic flows from Mach 0.8 to Mach 21, and covers a large range of Reynolds numbers from 10^2 up to 10^5 for a reference length of 100 mm (corresponding to the length of the flat plate used as a model). These flow conditions reconstitute most of the reentry vehicles' flight corridors from 140 km to 67 km of altitude, making this facility

unique in Europe. **Figure 10** exhibits the facility which can be divided in three parts: the settling chamber with a diameter of 1.3 m and a length of 2.0 m, the test chamber with a diameter of 2.3 m and a length of 5.0 m, and a third chamber in which a diffuser is installed and connects the pumping group to the facility through a vacuum gate. The pumping group is composed of 2 primary pumps, 2 intermediary Roots blowers, and 12 Roots blowers. Its performance makes it able to ensure low-density flow conditions continuously.

In this study, the entry conditions are simulated by a flow at Mach 4 and a static pressure of 8 Pa corresponding to a geometric altitude of 72 km. **Table 1** compiles the overall operating conditions for each nozzle, where P represents the pressure, T the temperature, ρ the volumetric mass density, U the flow velocity, M the Mach number, λ the mean free path, and Re the Reynolds number based on the flat plate length L = 100 mm and calculated with the relation $Re = U_1 L/\nu_1$, where ν is the kinematic viscosity in m^2/s because $\nu = \mu/\rho$. The air flow distribution is uniform through the test sections with a core diameter of 8 cm and a core length of 20 cm. Previous work had been undertaken with a flow at Mach 2 and a static pressure of 8 Pa corresponding to a geometric altitude of 67 km[21].

The model under investigation is a flat plate (50 mm-long, 80 mm-wide and 4 mm-thick) with a sharp leading edge (15°), as shown on **Figure 1**. The plasma actuator induces very high wall temperatures and thus, models must be manufactured in a heat-resistant material. The flat plates are made of quartz and the position of the model in the test chamber is sketched on **Figure 5**. The two electrodes setting the plasma actuator are manufactured in aluminum and designed with the following dimensions: 50 mm-width, 35 mm-length, and 80 µm-thickness. These electrodes are flush mounted on the upper surface of the flat plate. Depending on the nozzle, the core of the generated flow will have specific dimensions and the models must be adapted to these cores. Therefore, the width of the model strongly depends on the studied flow. However, to maintain a certain level of coherence, the ratio of the active electrode on the surface of the model is kept at 35%. The electrode located closest to the leading edge is defined as the cathode, or active electrode, and is connected to a high voltage DC power supply through a current limiting resistor (R_s = 10.6 kΩ) while the second electrode is grounded. The DC power supply is voltage-regulated and delivers the discharge current I_{HV} corresponding to the chosen V_s voltage. The voltage applied to the active electrode, V_{HV}, is then calculated with the following relation: $V_{HV} = V_s - R_s I_{HV}$. V_s and I_{HV} are read directly on the power supply. This procedure ensures the stability of the discharge conditions.

The adequate operation of the supersonic wind tunnel MARHy is based on accurate measurements of the stagnation and test section pressures. Capacitive sensors are used to measure the stagnation pressure, P_0, and the static pressure, P_1, and the pressure above the flat plate when combined to a Pitot probe. The Pitot tube is a flat-ended tube made of glass to avoid electrical interactions with the discharge. Its dimensions are D = 6 mm for the external diameter and d = 4 mm for the internal one (see **Figure 7** that shows the Pitot tube above the flat plate at position X = 50 mm, Y = 0 mm, Z = 0 mm which corresponds to the middle of the flat plate). The pressure mapping above the plate is ensured with a 3-axis traversing system, controlled by a computer. The step resolution of the Pitot probe on each axis is 0.1 mm ± 0.02 mm for each

position.

A MKS control unit with a 12-bit resolution is linked to the manometers associated to P_0 and P_1, whereas a MKS control unit is used for the Pitot probe acquisition. The 10 V output of each MKS control unit is read by an acquisition card storing the pressures values during experiments. **Figure 8** exhibits the manometers' positions.

An iCCD camera (1024 x 1024-pixel array) equipped with a VUV (Visible-Ultraviolet) objective lens (94 mm, *f* =4.1) is used for the flow visualization. As shown in **Figure 8**, the iCCD camera is placed perpendicular to the flow axis and collects light through a fluorine window located in the wall of the test section chamber.

An infrared camera is placed on the top of the wind tunnel focusing on the model through a zinc selenide (ZnSe) window compatible with the IR wavelength range of the camera, as drawn on **Figure 8**. This device follows and records the live evolution of the surface temperature of the model. The IR camera is equipped with a QWIP-type (Quantum Well Infrared Photodetector) IR photo-detector composed of a 320 x 240 pixel array.

First, the baseline is defined. It corresponds to the flow behavior around the model without any actuation. The flow conditions are detailed in **Table 1**. **Figure 9** presents the images of the baseline recorded with the iCCD camera and visualized using the luminescent discharge technique. The software ImageJ was used to improve the image contrast and thus, allowed a more precise determination of the shock wave. For this flow at Mach 4 for a static pressure of 8 Pa, the shock is sharp and attached to the leading edge of the flat plate. Therefore, the shock wave shape is fitted by a linear equation and a shock wave angle of $\beta = 23.2° \pm 0.5$ is detected.

The experimental and numerically normalized Pitot profiles are displayed on the same plot in **Figure 11** to calibrate the experimental profiles and confirm their validity. The normalization is made with the value of the maximum Pitot pressure of each profile. The profiles are plotted for the abscissa X = 50 mm (in the middle of the flat plate). Indeed, the Pitot pressure gradients are higher as distance increases from the leading edge as the gas compression due to the shock wave has a triangle shape. Therefore, it is easier to compare the profiles if the gradients are large enough. The knee visible on the profiles represents the shock transition where the shock wave and the boundary layer are merged.

As was observed, the experimental profiles were in good agreement with those calculated with the code. The shock wave angle was estimated with the position of the knee region, which gave an experimental shock angle of $\beta = 23.5° \pm 0.7°$, which was very similar to the value found with the iCCD images.

The discharge was created by applying a negative DC potential to the active electrode. **Figure 12** shows the current–voltage (I_{HV}–V_{HV}) characteristics of the plasma actuator. The discharge ignited at the voltage V_{HV} = -0.40 kV. The discharge current increased with the applied voltage, corresponding to the abnormal glow discharge regime. **Figure 13** shows a picture of the

discharge. The plasma has the shape of a flame and goes straight upward. It is assumed that as the static pressure is low, the plasma is very diffuse and is created between the cathode and the top of the experimental chamber instead of the grounded electrode. The plasma can easily be divided in two parts, a bright one, the negative glow, and a dark one, known as the cathodic or plasma sheath. When increasing the discharge power, the shock wave is pushed away and thus, the shock wave angle increases as shown in **Figure 14** where the shock waves are presented for two different discharge powers. **Figure 15** shows the variation of the shock wave angle with the discharge current. One can observe that the higher the discharge current, the higher the increase in the shock wave angle. Knowing that the shock wave angle is inversely proportional to the Mach number, it can be deduced from this result that the Mach number of the flow over the model decreases when switching on the discharge and gets even lower when increasing the discharge power.

Figure 1: Scheme of the plasma actuator mounted on the flat plate.
Figure 1 shows a scheme of the positions on the model and sizes of the electrodes constituting the plasma actuator.

Figure 2: Top view of the flat plate with the hole positions.
Figure 2 gives the positions and dimensions of the holes for the cable connections and the curvature radius of the electrodes.

Figure 3: Top view of the flat plate with the black painted lines for the IR camera.
Figure 3 shows an overview of the positions of the black painted lines drawn on the flat plate to allow better temperature detection with the IR camera.

Figure 4: Photo of the experimental setup in the test chamber.
Figure 4 illustrates the different elements in the test chamber with a picture. The nozzle, the flat plate on the standing pole, and the diffuser can be distinguished.

Figure 5: Experimental set-up.
Figure 5 is a schematic of the whole experimental setup with the direction of the axis, the position of the power supply connections, and the flow direction.

Figure 6: Scheme of setting up the angle of attack.
Figure 6 helps in understanding how to set up an angle of attack for the model with the standing pole.

Figure 7: iCCD image of the Pitot tube located in the middle of the flat plate (X=50 mm, Y=0 mm, Z=0 mm).
Figure 7 is a picture of the Pitot tube above the flat plate and allows the understanding of the Pitot design.

Figure 8: Schematic view of the wind tunnel and configuration of the diagnostics.
Figure 8 shows the positions of the different diagnostics such as the iCCD camera, the

manometers, and the IR camera.

Figure 9: Experimental baseline flow field obtained with the iCCD images.
Figure 9 is an improved iCCD image of the baseline obtained with the luminescent technique. It demonstrates the shock wave obtained for the flat plate in a Mach 4 flow at a static pressure of 8 Pa.

Figure 10: The MARHy wind tunnel layout.
Figure 10 is a 3D layout of the MARHy wind tunnel which details the three main parts: the settling chamber, the test chamber, and the diffuser. It gives the parameters linked to each of these parts.

Figure 11: Numerical and experimental Pitot probes profiles at X = 50 mm for the baseline case.
Figure 11 is a plot exhibiting the numerical and experimental Pitot probe profiles at X = 50 mm for the baseline case. This figure is used to validate the experimental profile and confirm the determined shock wave angle.

Figure 12: Current-voltage characteristics of the plasma actuator.
Figure 12 illustrates the discharge current corresponding to the applied discharge voltage. This figure aids in understanding the performance of the plasma actuator and its energy consumption.

Figure 13: Picture of the flat plate with discharge fired.
Figure 13 is a picture of the plasma created above the flat plate when the plasma actuator is on and the flat plate is placed in the Mach flow at a static pressure of 8 Pa.

Figure 14: Picture of the flat plate with the discharge fired for two different discharge currents.
Figure 14 exhibits the shock wave modifications obtained for two different discharge currents on the same picture to illustrate the effect of the plasma actuator on the shock wave angle when increasing the discharge current.

Figure 15: Dimensionless shock wave angles versus the discharge current per unit of surface.
Figure 15 is a plot of the dimensionless shock wave angles versus the discharge current per unit of surface. It shows the increase of the shock wave angle with the discharge current.

Figure 16: Temperature profiles along the X-axis of the flat plate.
Figure 16 illustrates the evolution of the temperatures along the X-axis of the flat plate for different power discharge settings. It shows the particular shape of the temperature profiles and the temperature values demonstrating that the surface heating is negligible.

Figure 17: Effect of the plasma discharge on the Pitot probe profiles measured at X = 50 mm.
Figure 17 illustrates the Pitot pressure profiles above the middle of the flat plate for different discharge currents. This plot demonstrates the increase in the knee height, confirming the shock wave angle increase. Furthermore, it shows the low increase of the boundary layer and thus, its low impact on the shock wave angle increase.

Figure 18: Estimation of the drag induced by the plasma actuator over the flat plate.
Figure 18 plots the drag coefficient versus the discharge power and demonstrates that it increases with the discharge power. This is related to the increase in the shock wave angle which also increases with the discharge power.

Figure 19: Effect of the plasma actuator on the entry guidance drag velocity profile.
Figure 19 demonstrates the effect of the plasma actuator overall on the entry guidance of a reentry vehicle. Indeed, in the first phase of the reentry for a given velocity, if the drag is increased +13% with the plasma actuator, it would give a lower effective velocity.

Table 1: Operating conditions.
Table 1 shows the main parameters of the flow studied in this paper as the Mach number, the Reynolds number, or the static pressure.

DISCUSSION:
The described experimental protocol presents some critical steps. The first point concerns the repeatability of experiments because, for a given experimental condition, several experimental campaigns are needed. Indeed, to have a complete physical analysis, different diagnostics are used that cannot be applied simultaneously. This implies that the experimental set-up (model, electrode size and shape, position of the model in the test chamber, *etc.*) must be rigorously the same throughout the experiments. Even slight differences can induce different discharge conditions modifying the plasma actuator effects and prevent the results from being directly comparable. The other point directly impacts the shock wave angle measurements. Indeed, each iCCD image needs specific post-processing, and is analyzed manually. Therefore, it is essential to apply a well-run method for every post-processing. Furthermore, the shock wave angles are also determined from Pitot probe profiles and compared to angles detected with the iCCD images to strengthen the measurements.

The technique of utilizing plasma actuators also presents some issues. The main limitation of such actuators is due to the flow conditions, especially the pressure and, thus, the altitude of the atmospheric re-entry of the spacecraft. Plasma actuators have to be characterized in different flow regimes in terms of speed and pressure to extrapolate their behavior to real cases. For this purpose, it is necessary to deeply understand the plasma physics and its coupling with the flow to overcome these challenges. Some authors incriminated thermal effects (bulk and surface) for the shock wave modifications in supersonic conditions[22]. Shin *et al.* investigated thermal effects with two distinct discharge modes, where an increase in gas temperature was observed; nevertheless, no clear evidence of plasma effects on the flow was identified[15].

The present paper shows that other physical aspects related to the discharge, rather than thermal considerations, have to be taken into account to explain the flow modifications. **Figure 16** displays the temperature distributions along the longitudinal axis of the model. The plots show that the plasma actuator heats the surface of the model, although the distribution is non-uniform and the maximum values are found close to the leading edge. The non-uniformity is induced by variation in the electric field along the X-direction and this electric field is highest close to the

leading edge of the flat plate[23]. For a given value of the discharge current I_{HV}, the plasma discharge without the Mach 4 flow (static pressure set to 8 Pa) induced a similar heating of the flat plate, with a temperature distribution similar (both in value and shape) to the temperature distribution when the Mach 4 flow is operating. This result confirms that the heating of the flat plate surface is mainly related to a discharge effect and not influenced by the interaction between the Mach 4 air flow and the flat plate surface. Moreover, the surface heating induces a displacement effect: the flow viscosity above the heater is modified, inducing an increase in the laminar boundary layer thickness, and consequently, the shock wave is shifted outward from the flat plate surface (*i.e.*, the shock wave angle increases). This effect can be observed more clearly on **Figure 17** where four Pitot pressure profiles are presented: one corresponds to the baseline, and the others correspond to the cases when different discharge powers are supplied. On the shape of the profiles measured at X = 50 mm, the knee geometry is found at a higher position on the Z-axis, meaning that the thickness of the boundary layer has increased and therefore, the shock wave angle increased as well.

Experiments carried out with a Mach 2 flow and a static pressure of 8 Pa showed that the thermal effects accounted for only 50% of the shock wave angle increase and the remaining 50% of changes were due to ionization effects[21]. For Mach 2 and Mach 4 flows, the surface temperature distributions are similar, although the temperature gradients are higher with the Mach 2 flow. Therefore, one can assume that the ionization effect would be even greater with the Mach 4 flow than the 50% estimated in previous studies[21], meaning that the influence of surface heating on the shock wave modification will be even less important.

During atmospheric re-entries, atmospheric drag is used to slow down the vehicle, but the amount of energy to dissipate in these conditions is enormous. The rate of energy dissipation is then estimated to be proportional to the cube of the vehicle speed, inducing very high temperatures on the spacecraft which may produce serious damage if thermal protections are not sufficient. Optimal return trajectories are designed to obtain the minimum return cost defined as the sum of the mass propellant consumed by the space vehicle to de-orbit and the mass of thermal protections. However, reduction of thermal protection could be a way to decrease the cost of future missions. For this purpose, one idea is to increase the drag force with the aim of decelerating the vehicle, and the use of plasma actuators is a potential method to achieve this goal.

In order to estimate the efficiency of plasma actuators in heat load reduction, numerical simulations corresponding to the presented experimental conditions have been carried out to determine the aerodynamic drag forces induced by the discharge over a flat plate at Mach 2 and 8 Pa[2]. The surface heating produced by the plasma discharge is numerically simulated reproducing the shock wave angle modifications observed experimentally. Results showed that, with only the surface heating, the shock wave angles are half those determined with the plasma actuator. The drag force was then calculated from the surface pressure gradient obtained for each experimental condition. An empirical law was obtained, linking the shock wave angle and the drag coefficient based on the effect of the surface heating. An extrapolation of this law allowed the determination of the drag coefficients corresponding to the shock waves angles

obtained with the plasma actuator. **Figure 18** presents the behavior of the drag coefficient with the discharge power applied to the plasma actuator. An increase of 13% for the drag coefficient is expected in our experimental conditions when applying 78.3 W to the plasma actuator. For the re-entry of a space shuttle in the mold of Columbia, a rough estimation of the drag increase impact can be obtained from the entry guidance drag velocity profile[24]. **Figure 19** presents the space shuttle re-entry guidance in terms of drag acceleration, as a function of the relative velocity, for the real trajectory and for the trajectory with an increase of 13% for the drag coefficient. The shift of the new trajectory shows that the shuttle velocity decreases about 7% for velocities around 7 km/s corresponding to the beginning of the atmospheric entry. As the heat flow is proportional to the power 3.15 of the shuttle speed, the speed has a drastic influence on the heat flow, leading to a decrease of 26% of the heat flow through 1 m^2/s of the Space Shuttle surface at the stagnation point[25]. Taking into account that the mass of the heat protection in the shuttle is of 9,575 kg and that the decrease in the heat flow is proportional to the mass protection[25], 2.5 tons of the shuttle mass could be saved with a plasma actuator. In future applications, the plasma actuators could even be extended to control a full trajectory.

ACKNOWLEDGMENTS:

The authors acknowledge the French Government's Investissement d'Avenir program: Laboratoire d'Excellence CAPRYSSES (grant no. ANR-11-LABX-0006-01). Additional funding is provided by the Région Centre with the PASS grant (convention no. 00078782).

The authors would furthermore like to acknowledge the constructive feedback from the reviewers.

DISCLOSURES:

The authors have nothing to disclose.

REFERENCES:

1. Sellers, J. J., Astore, W. J., Giffen, R. B., Larson, W. J. *Understanding space: An introduction to astronautics*. *Primis* (2000).
2. Coumar, S., Joussot, R., Parisse, J.-D., Lago, V. Influence of a plasma actuator on aerodynamic forces over a flat plate interacting with a rarefied Mach 2 flow. *IJNMHFF*. **26** (7), 2081 – 2100, DOI:10.1108/HFF-07-2015-0285 (2016).
3. Joussot, R., Coumar, S., Lago, V. Plasmas for High Speed Flow Control. *Aerospace Lab*. **10,** DOI:10.12762/2015.AL10-04 (2015).
4. Kimmel, R. L., Hayes, J. R., Menart, J. A., Shang, J. Effect of surface plasma discharges on boundary layers at mach 5. *AIAA Paper*. **0509** (2004).
5. Kuo, S. P., Bivolaru, D. The similarity of shock waves generated by a cone-shaped plasma and by a solid cone in a supersonic airflow. *Phys. Plasmas*. **14** (2), 023503-023508 (2007).
6. Kuo, S. P. Plasma mitigation of shock wave: experiments and theory. *Shock Waves*. **17** (4), 225-264 (2007).
7. Leonov, S. B., Yarantsev, D. A., Gromov, V. G., Kuriachy, A.P. Mechanisms of flow control by near-surface electrical discharge generation. *AIAA Paper*. **780** (2005).
8. Leonov, S. B., Yarantsev, D. A. Near-surface electrical discharge in supersonic airflow: Properties and flow control. *J. Propul. Power*. **24** (6), 1168–1181 (2008).

9. Leonov, S. B. Review of plasma-based methods for high-speed flow control. *AIP Conf. Proc*. **1376**, 498–502 (2011).
10. Starikovskiy, A., Aleksandrov, N. Nonequilibrium Plasma Aerodynamics. *Aeronautics and Astronautics INTECH Open Access Publisher* (2011).
11. Cahn, M. S., Andrew, G. M. Electrodynamics in supersonic flow. *AIAA 6th Aerospace Sciences Meeting* (New York) (1968).
12. Roth, J. R. Physics and phenomenology of plasma actuators for control of aeronautical flows. *J. of Phys. D*. **40** (3) (2007).
13. Bletzinger, P., Ganguly, B. N., Van Wie, D., Garscadden, A. Plasmas in high-speed aerodynamics. *J. of Phys. D*. **39**, 33-57 (2005).
14. Fomin, V. M., Tretyakov, P. K., Taran, J. P. Flow control using various plasma and aerodynamic approaches. *Aerospace Sci. and Tech.*, **8**, 411-421 (2004).
15. Shin, J., Narayanaswamy, V., Raja, L. L., Clemens, N. T. Characteristics of a plasma actuator in Mach 3 flow. *In 45th AIAA Aerospace Sciences Meeting and Exhibit* (Reno) (2007).
16. Poggie, J., Adamovich, I., Bisek, N., Nishihara, M. Numerical simulation of nanosecond-pulse electrical discharges. *PSST*. **22** (1), 015001 (2012).
17. Schaaf, S.A. The Pitot probe in low-density flow. *AGARD*, **525** (1966).
18. Potter, J., Kinslow, M., Boylan, D. An influence of the orifice on measured pressures in rarefied flow. *Rarefied Gas Dynamics, **2***, 175 (1965).
19. Potter, J. Techniques Expérimentales Liées à l'Aérodynamique à Basse Densité. *AGARD*, **318** (1990).
20. Allègre, J. The SR3 low density wind tunnel-Facility capabilities and research development. *28th Joint Propulsion Conference and Exhibit*. 3972 (1992).
21. Joussot, R., Lago, V., Parisse, J.-D. Quantification of the effect of surface heating on shock wave modification by a plasma actuator in a low-density supersonic flow over a flat plate. *Experiments in Fluids*, **56** (5), 102 (2015).
22. Semenov, V. E., Bondarenko, V. G., Gildenburg, V. B., Gubchenko, V. M., & Smirnov, A. I. Weakly ionized plasmas in aerospace applications. *Plasma physics and controlled fusion*, **44**(12B), B293 (2002).
23. Parisse, J.-D., Léger, L., Depussay, E., Lago, V., Burtschell, Y. Comparison between Mach 2 rarefied airflow modification by an electrical discharge and numerical simulation of airflow modification by surface heating. *Physics of Fluids*, **21** (10), 106103 (2009).
24. Hale, W., Chapline, G. Wings In Orbit. *Education*, **9**, 20 (2010).
25. Bolonkin, A. A new method of atmospheric reentry for space shuttle. *AIAA Paper*, **2006-6985**, 6-9 (2006).

Figure1

Click here to download Figure Figure1.jpg

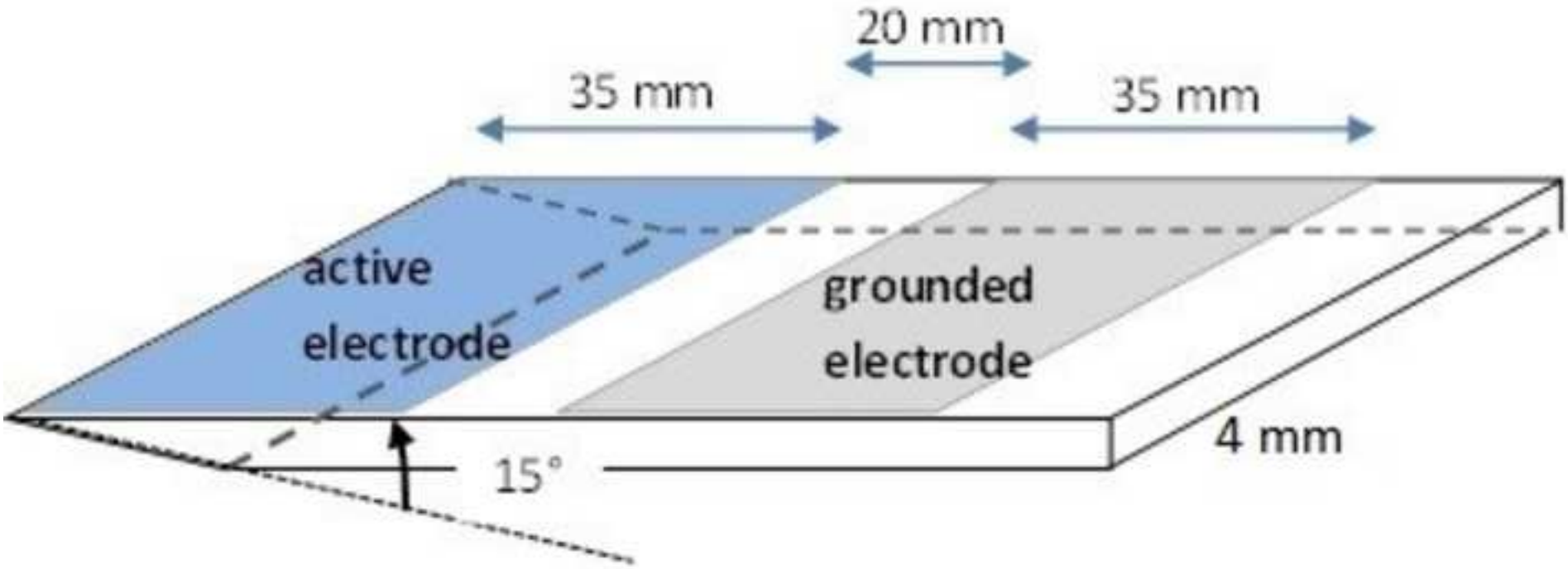

Figure2

Click here to download Figure Figure2.jpg

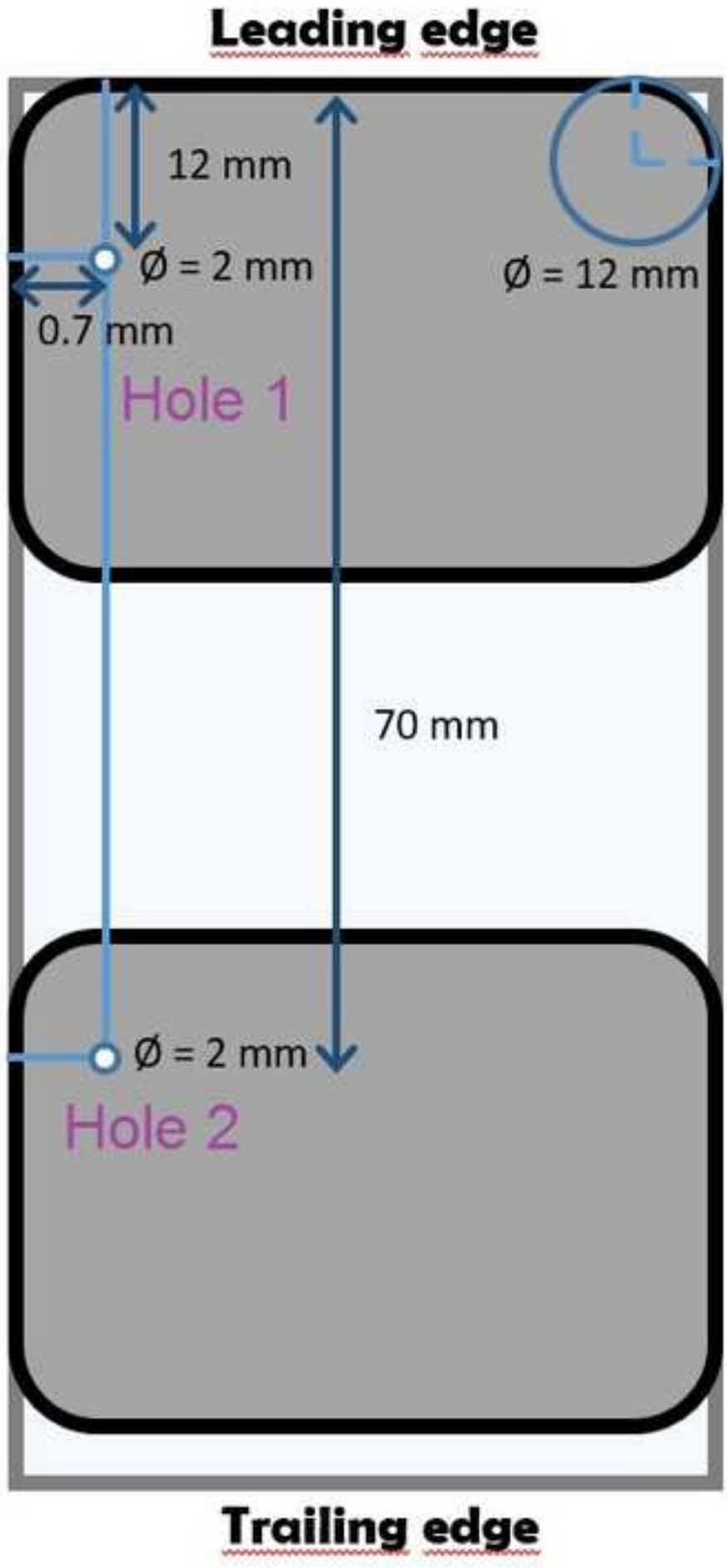

Figure3

Click here to download Figure Figure3.jpg

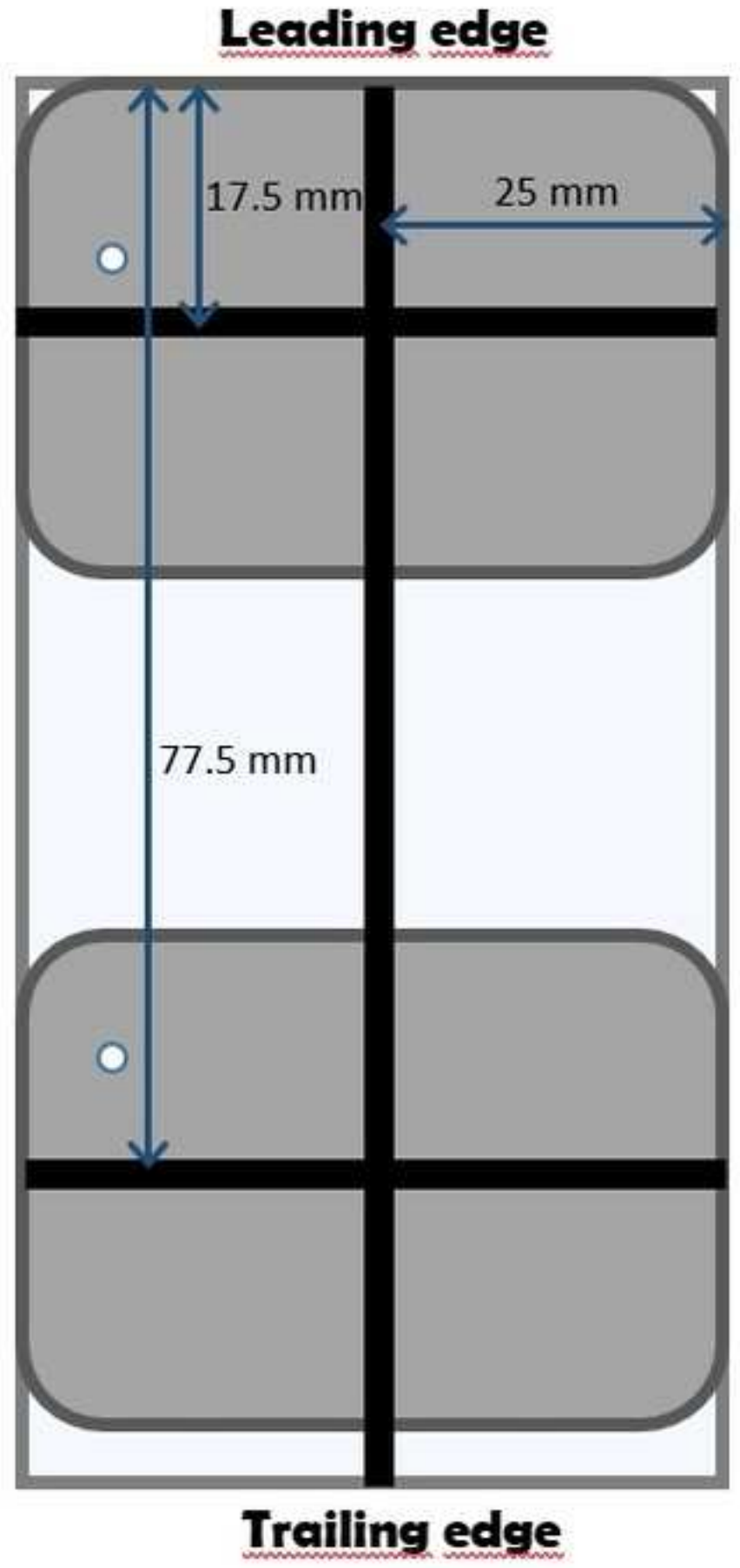

Figure4

Click here to download Figure Figure4.JPG

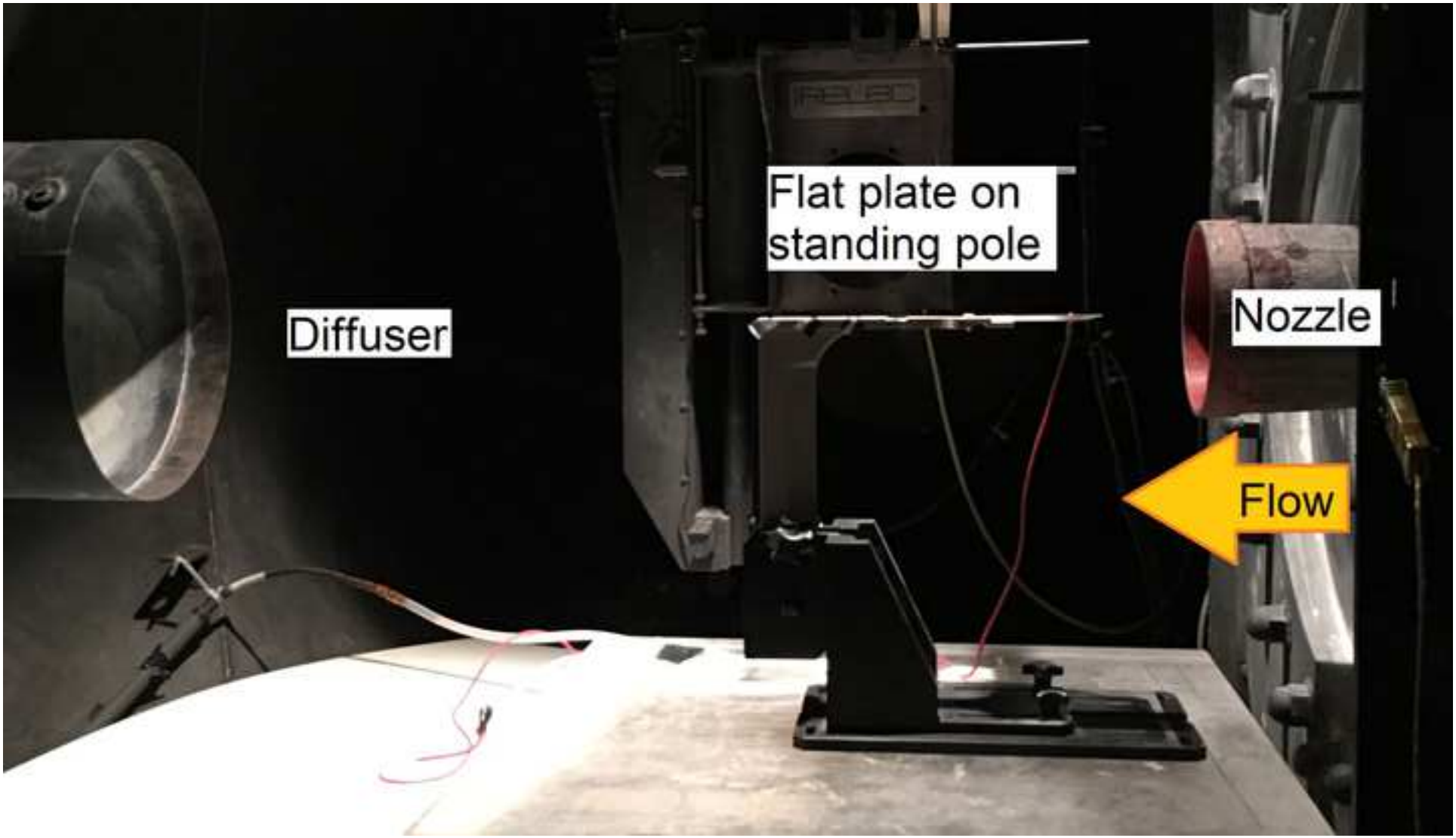

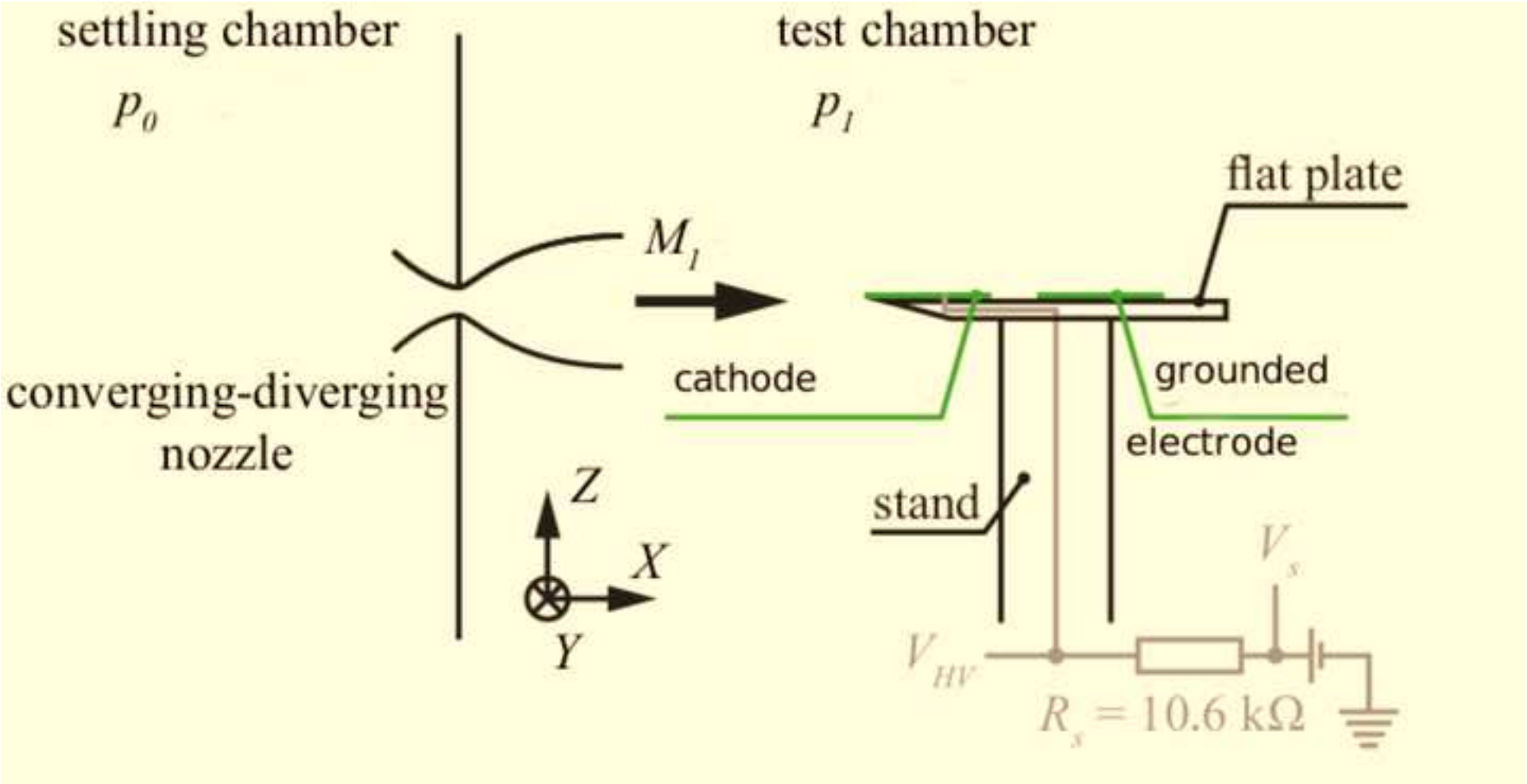

Figure6

Click here to download Figure Figure6.jpg

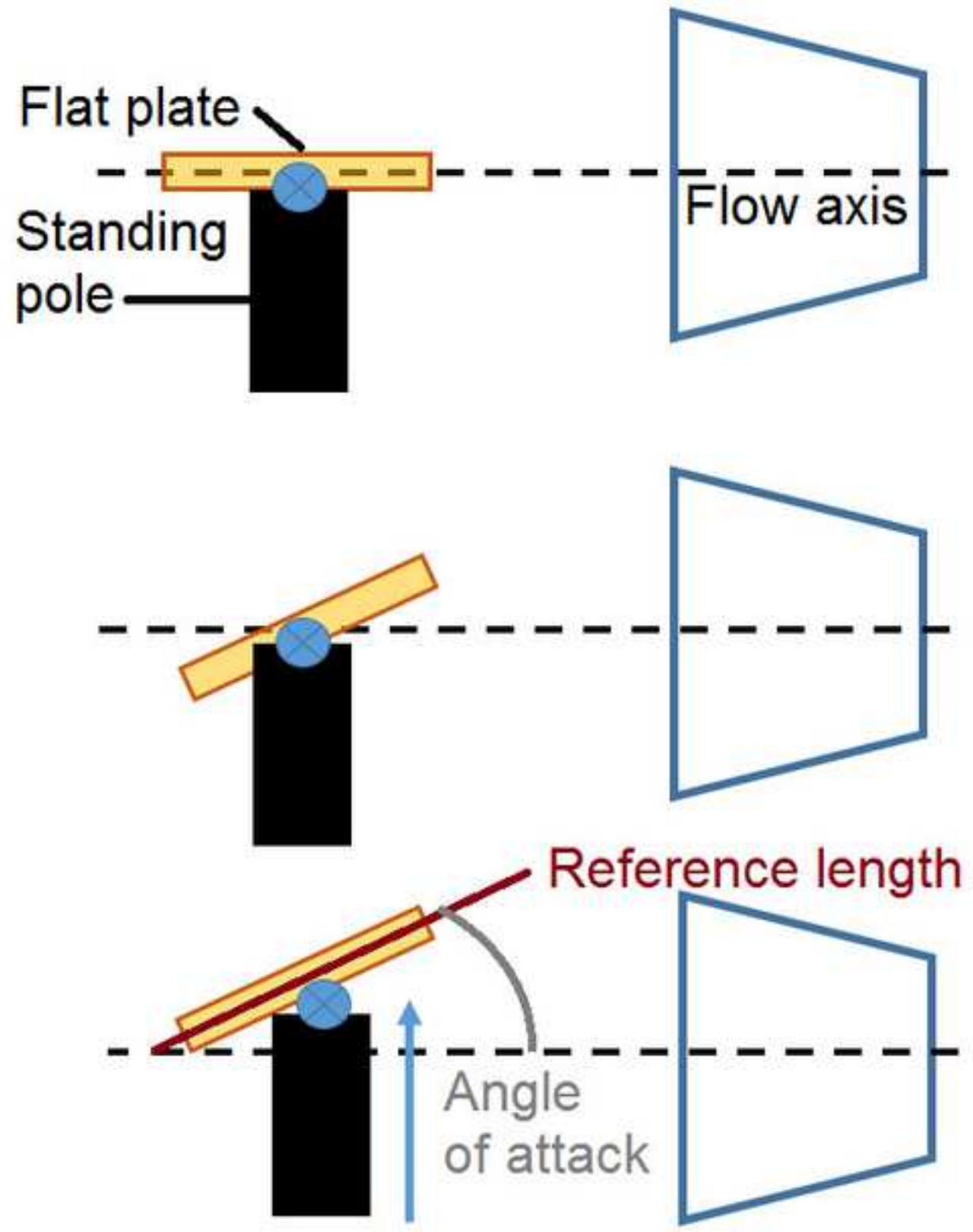

Figure7

Click here to download Figure Figure7.jpg

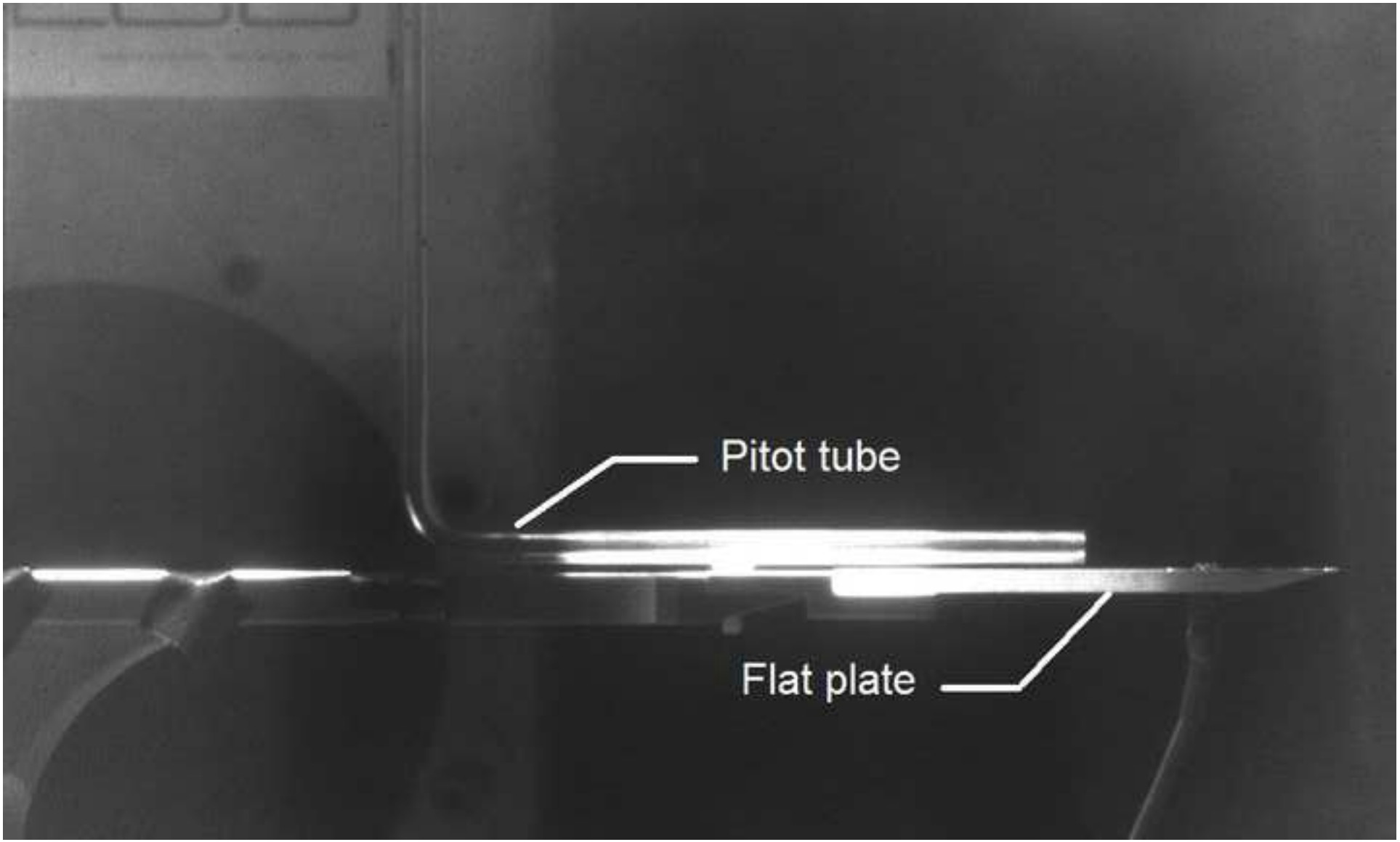

Figure8

Click here to download Figure Figure8.jpg

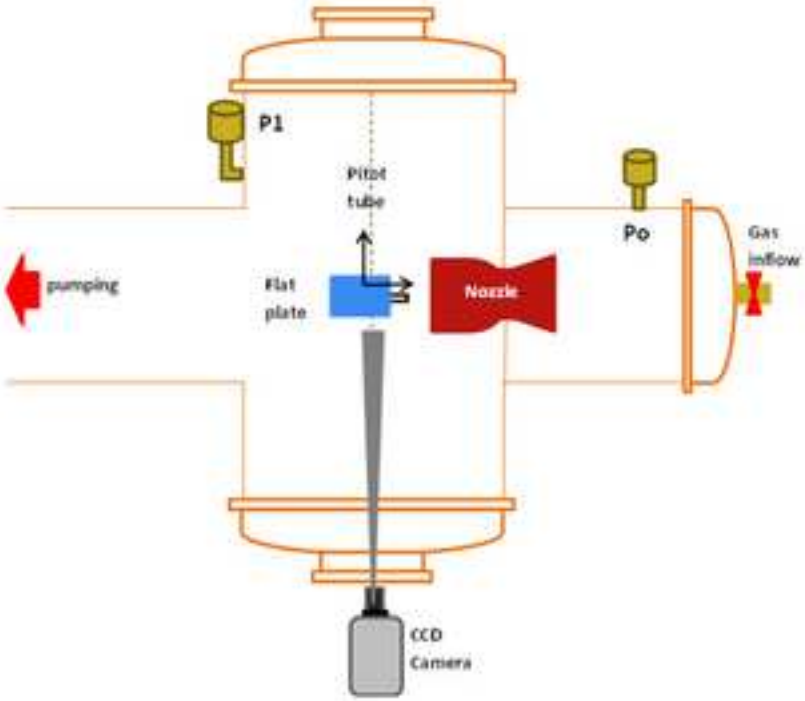

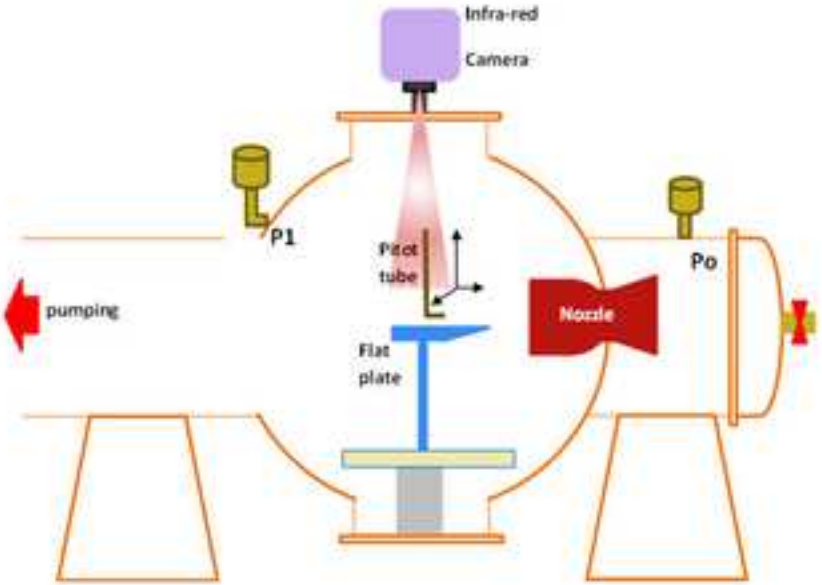

Figure9

Click here to download Figure Figure9.jpg

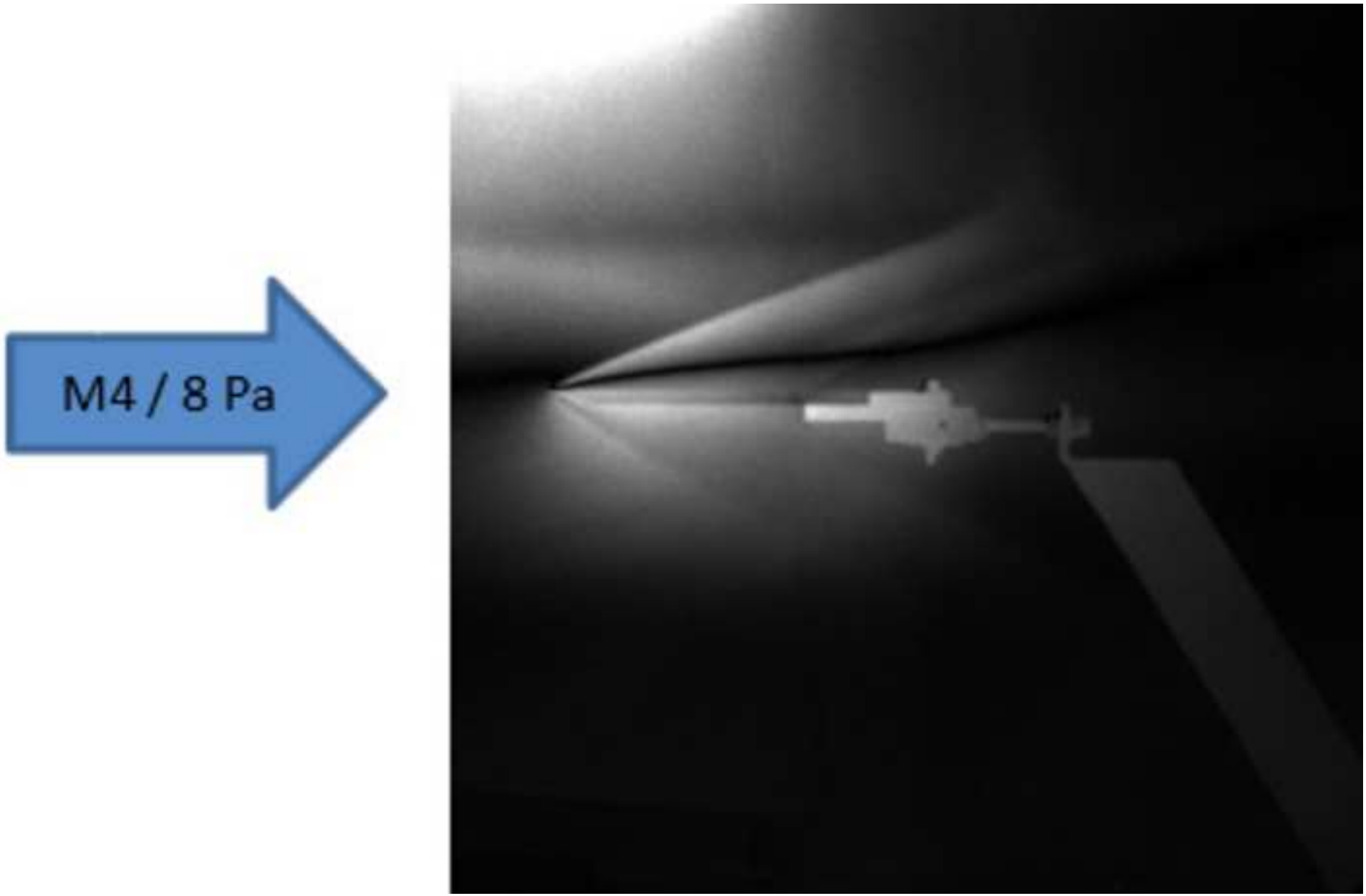

Figure10

Click here to download Figure Figure10.jpg

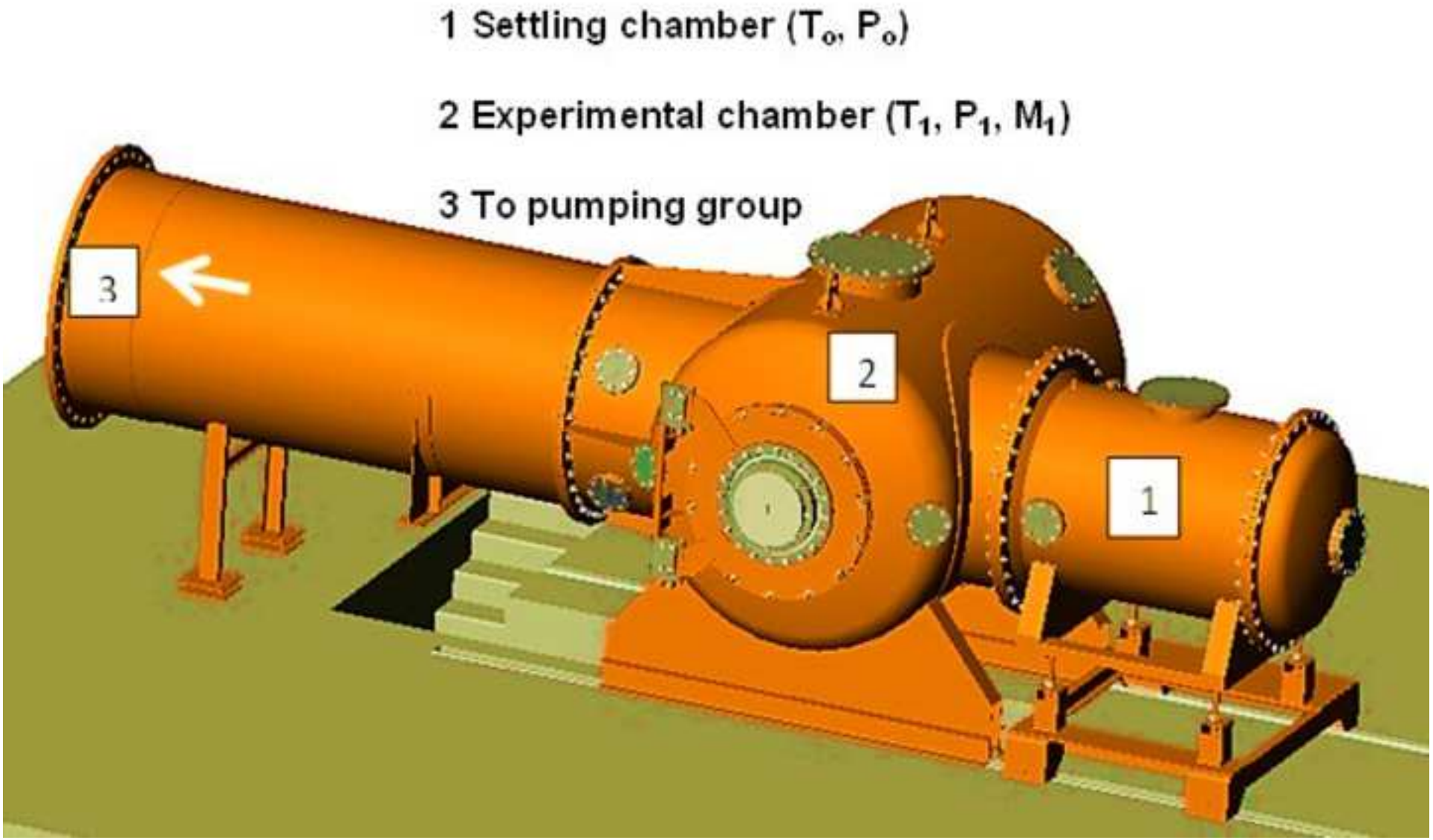

Figure11

Click here to download Figure Figure11.jpg

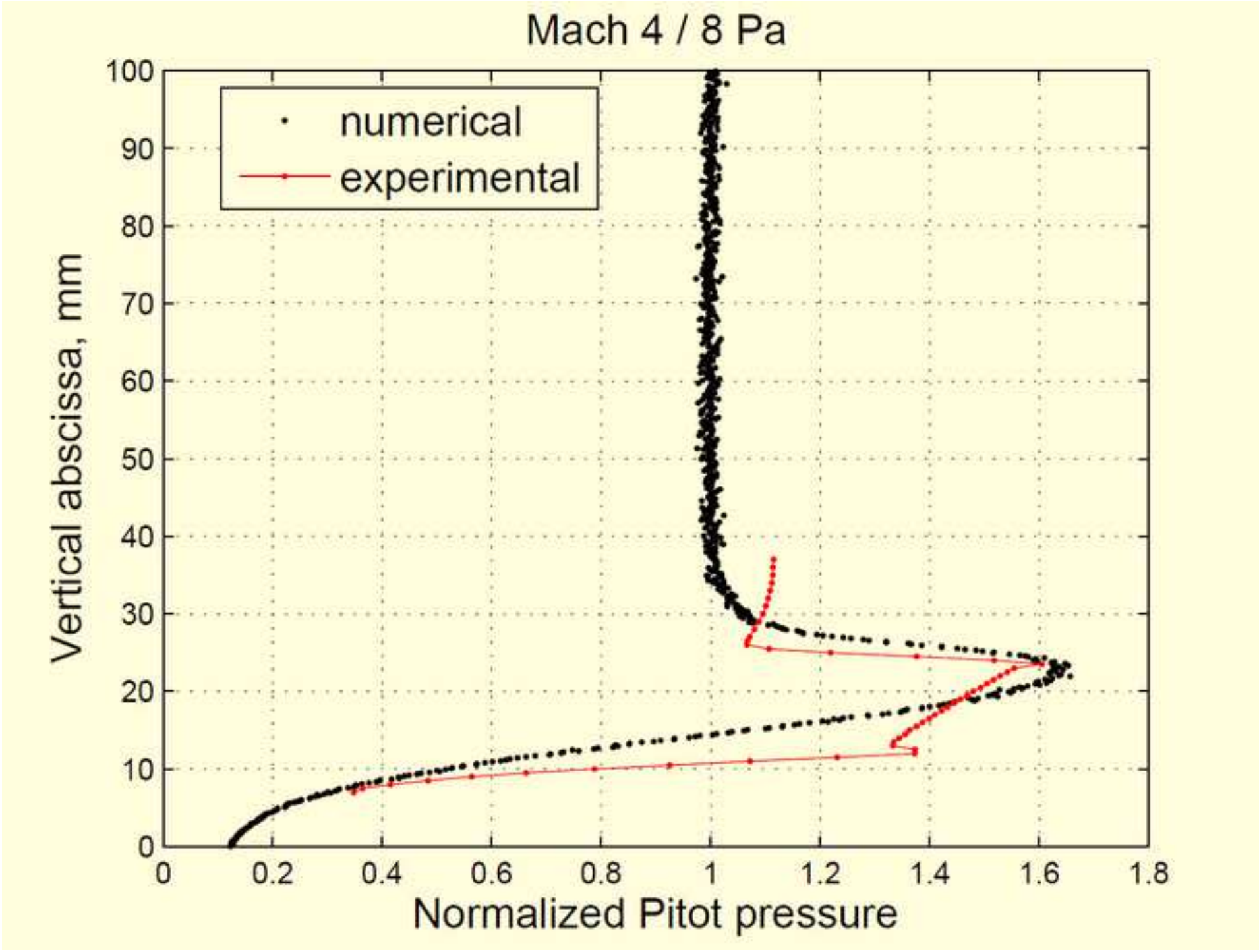

Figure12

Click here to download Figure Figure12.jpg

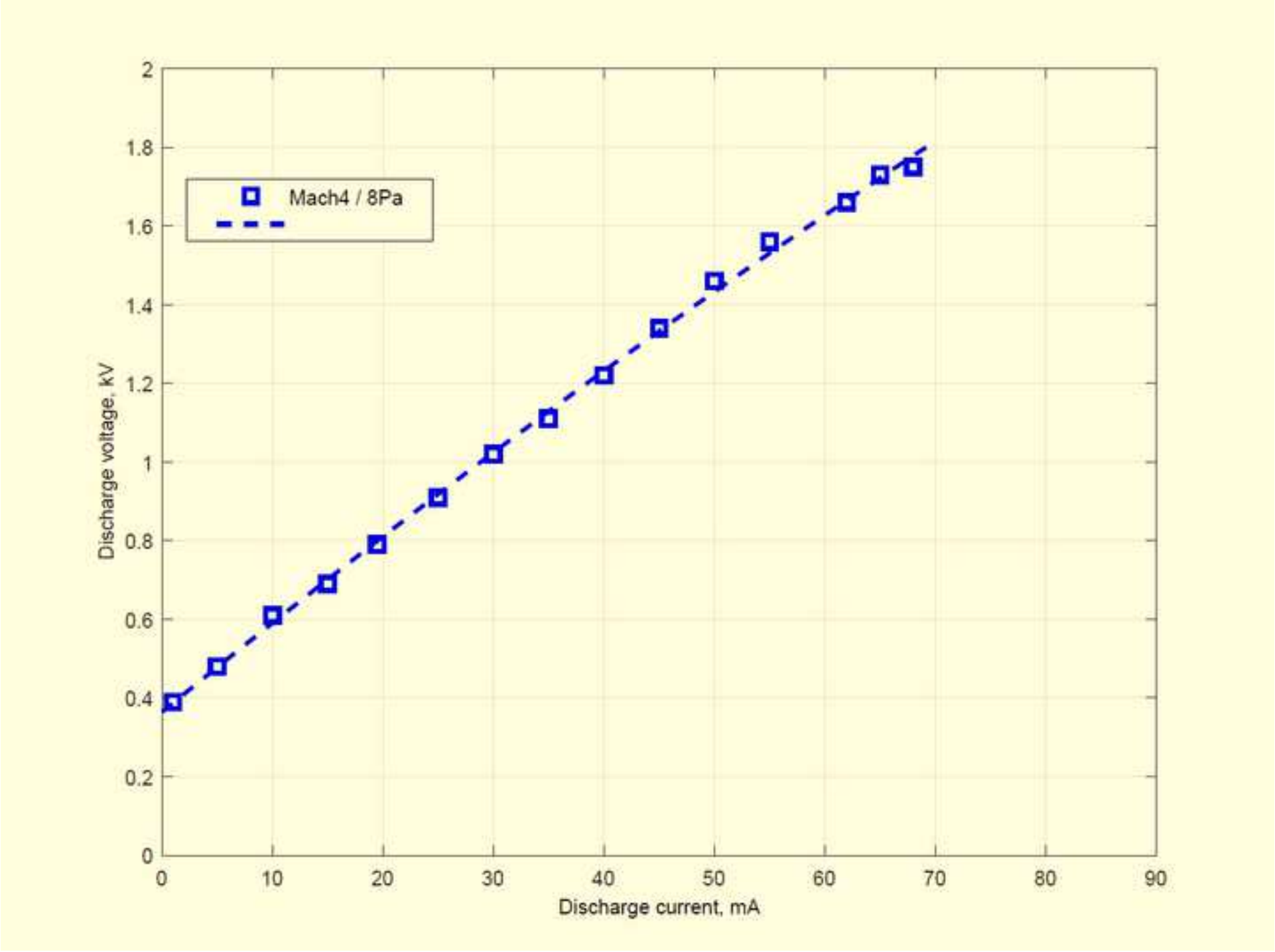

Figure13

Click here to download Figure Figure13.jpg

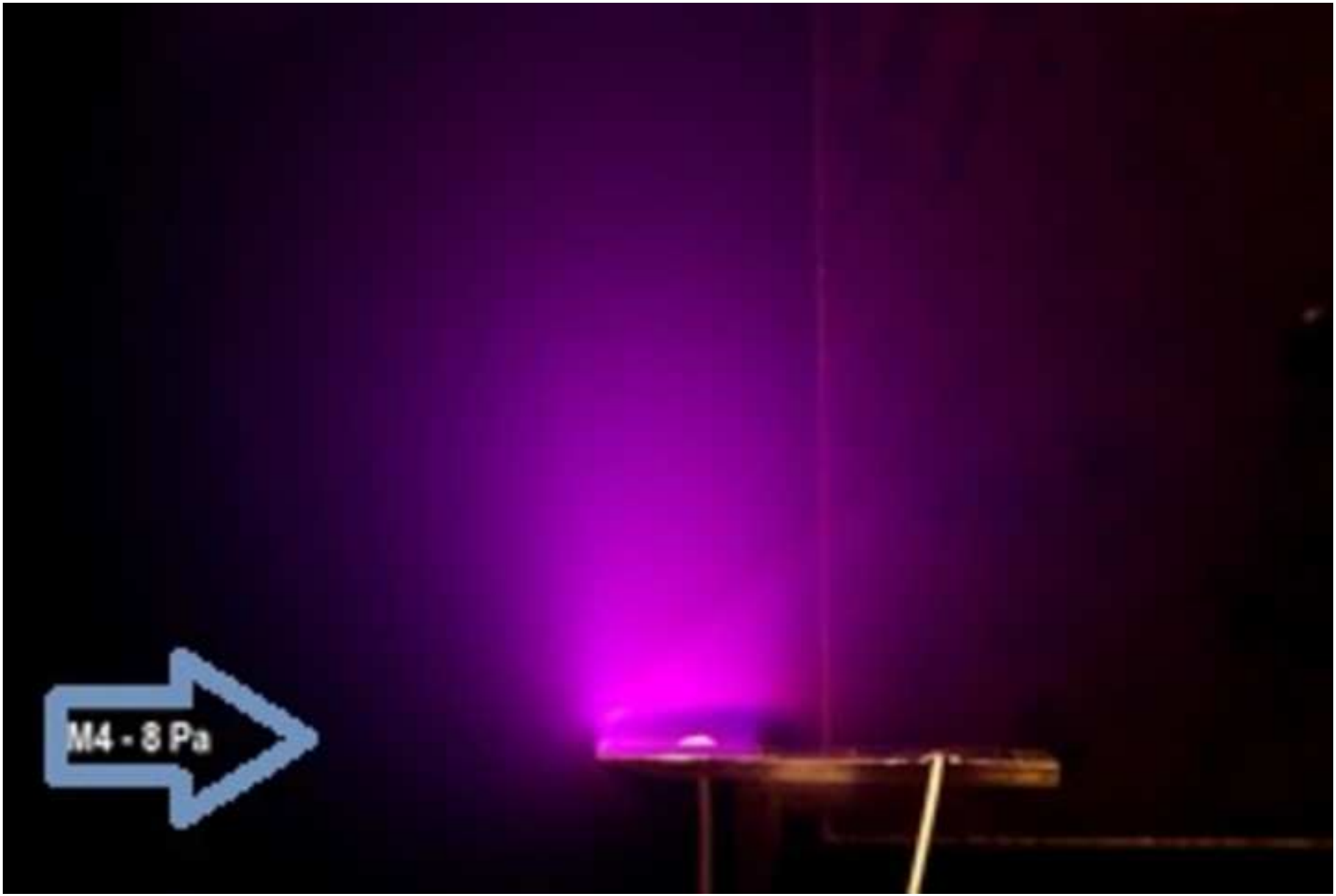

Figure14

Click here to download Figure Figure14.jpg

Figure15

Click here to download Figure Figure15.jpg

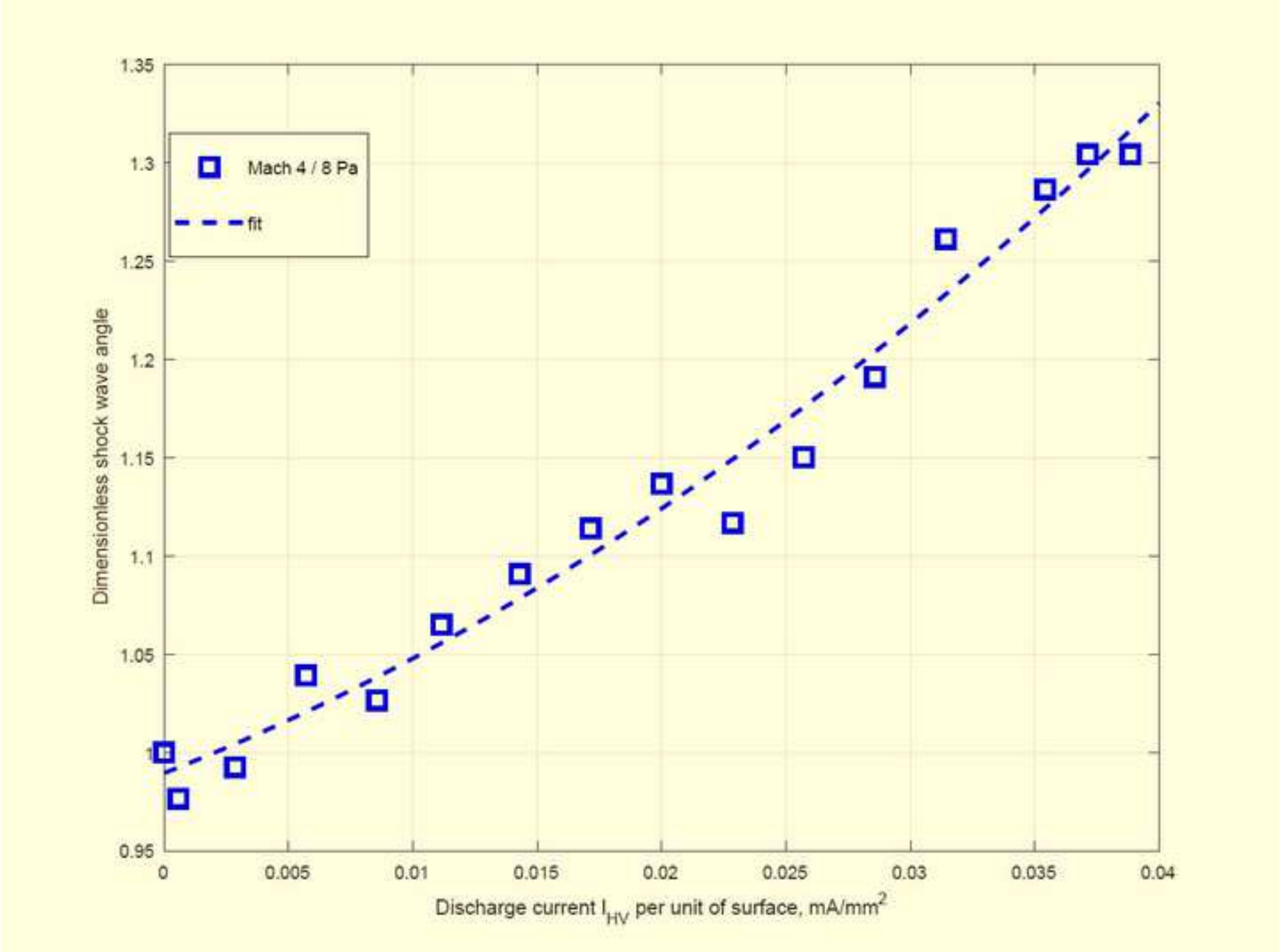

Figure16

Click here to download Figure Figure16.jpg

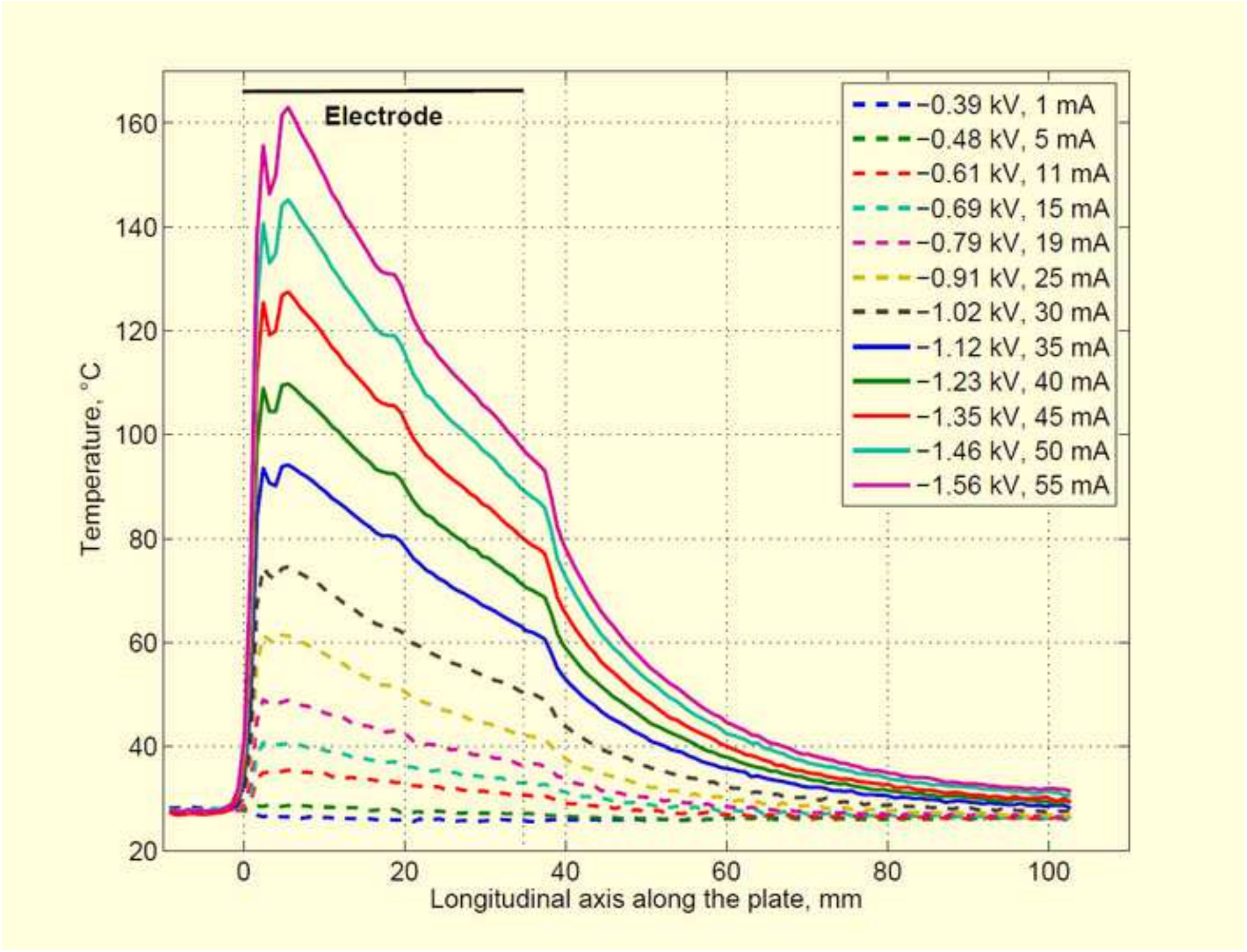

Figure17

Click here to download Figure Figure17.jpg

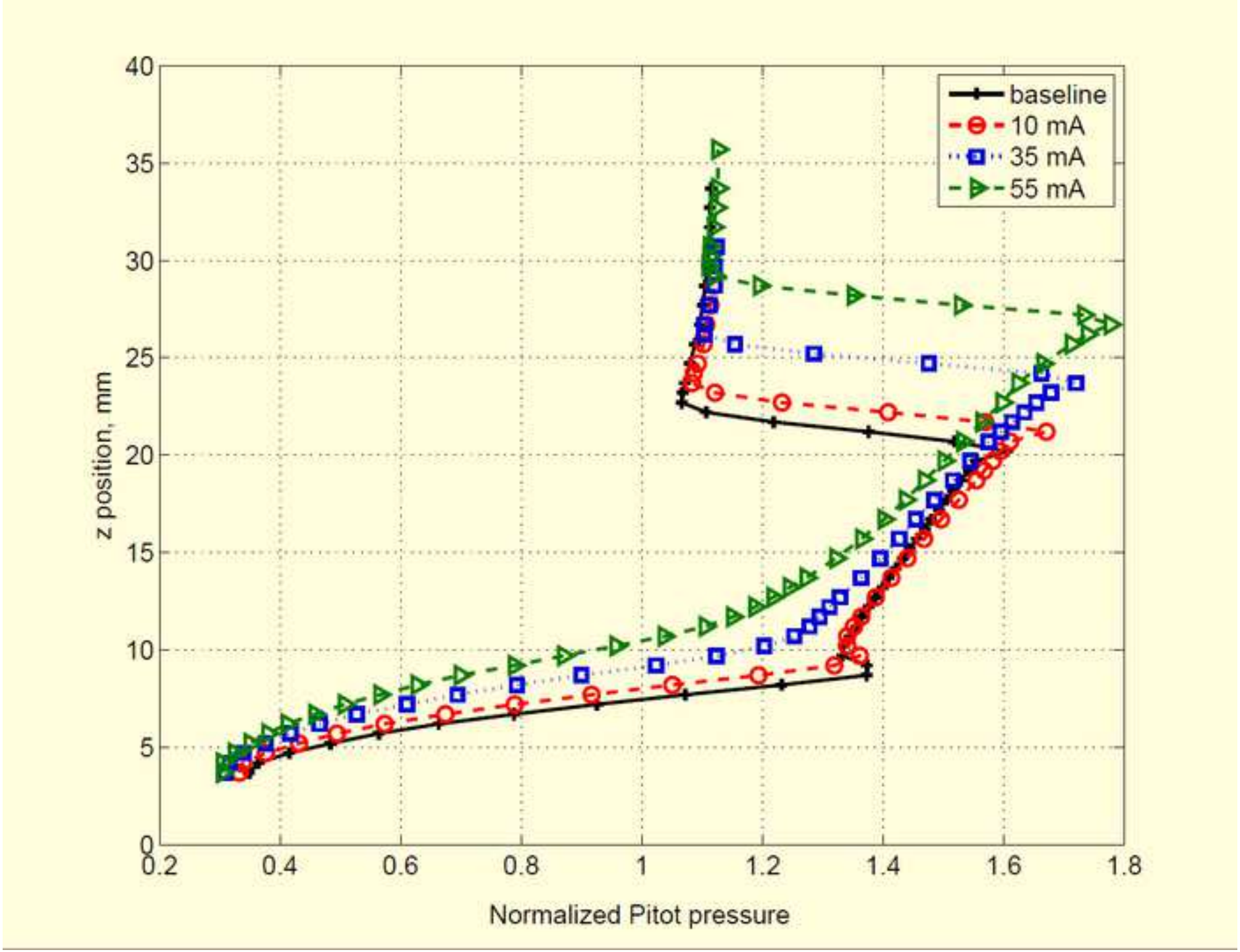

Figure18

Click here to download Figure Figure18.jpg

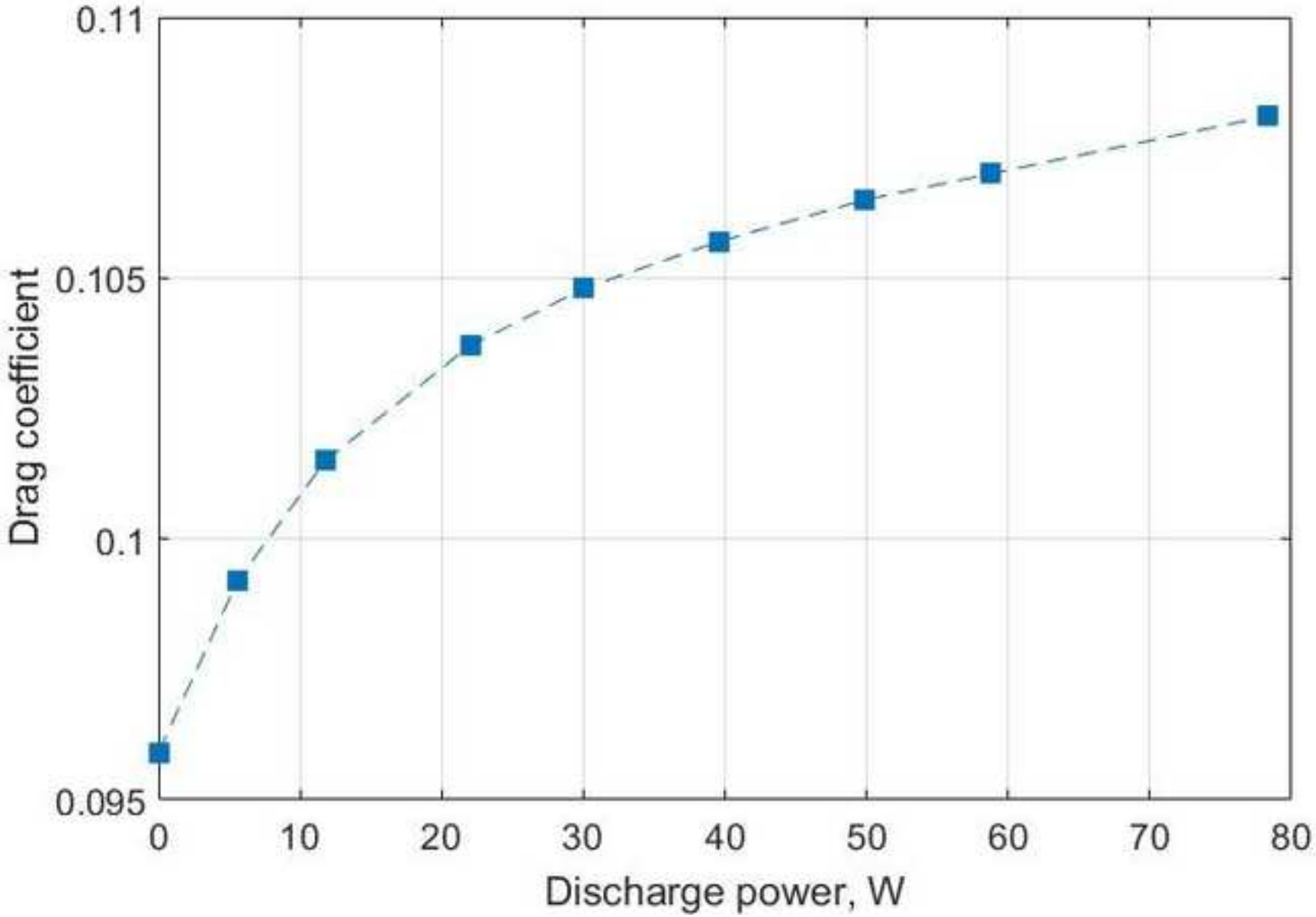

Figure19

Click here to download Figure Figure19.jpg

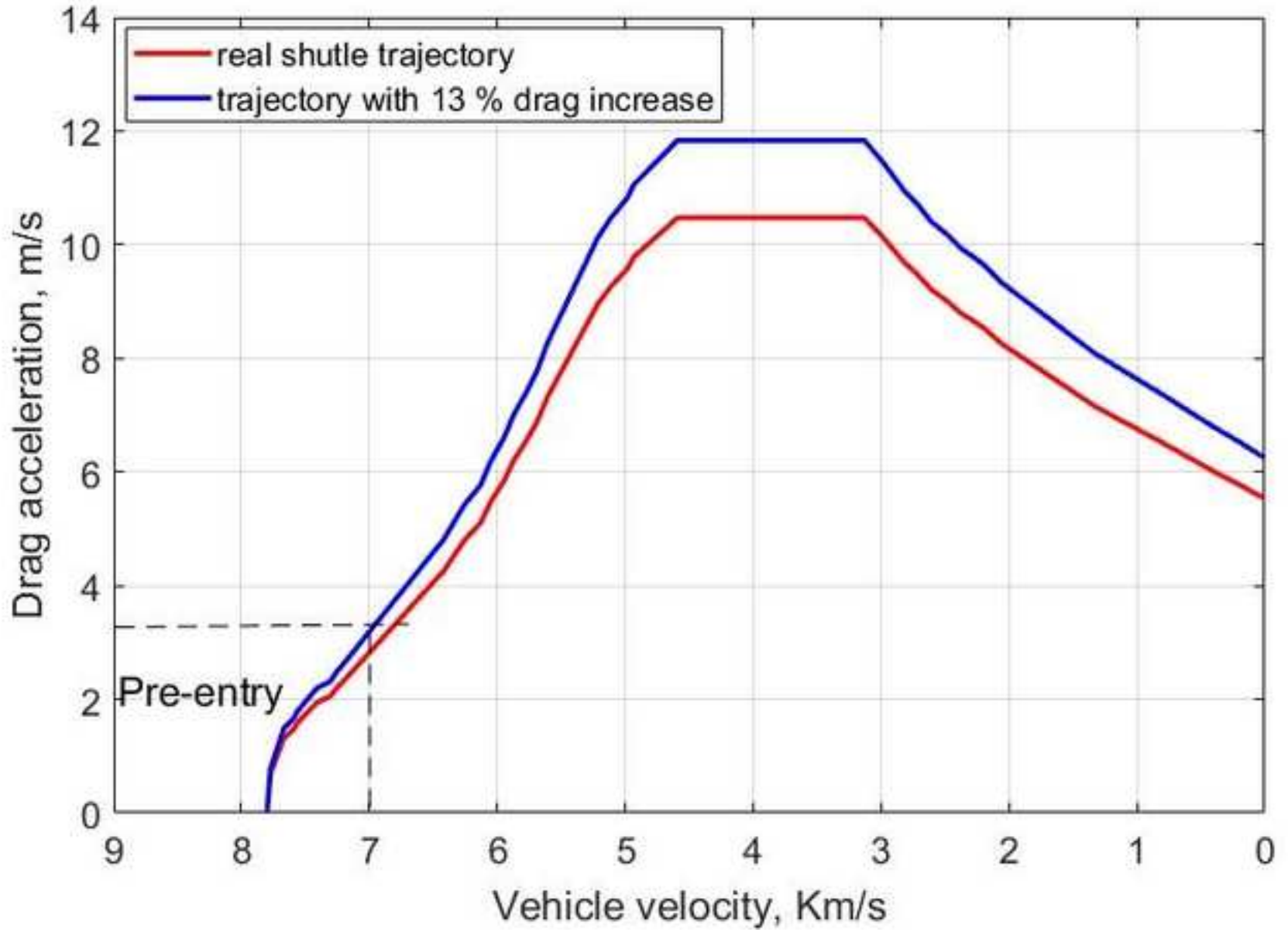

Animated Figure (video and/or .ai figure files)

Click here to access/download

Animated Figure (video and/or .ai figure files)

Montage2.gif

Table1

Stagnation conditions	Free stream conditions
P_0 = 1214 Pa	P_1 = 8 Pa
T_0 = 293 K	T_1 = 70 K
ρ_0 = 1.44x10^{-2} kg.m^{-3}	ρ_1 = 3.99x10-4 kg.m^{-3}
	μ_1 = 1.10x10^{-5} Pa.s
	U_1 = 670 m.s^{-1}
	M_1 = 4
	λ_1 = 0.067mm

Table of Materials/Equipment

Click here to download Table of Materials/Equipment JoVE_Materials.xls

Name of Material/ Equipment	Company	Catalog Number
Aluminium adhesive	Plasto Pro	212 16 763
Acetone	RS Pro	918-1082
RTV silicone glue	Permatex	800368
Kapton tape	Eurostat	42-020-0025
Quartz model	ALC Quartz	On request
Drill	Atelier La Trouvaille	MTA3
Thermocouple	RS Pro	XS-338-RS
DC Power supply	Spellman	SR15PN6
Motion controller	National Instruments	PXI-7344
iCCD camera	Princeton Instruments	GenII
IR camera	FLIR	ThermaCam SC 3000
Generating pressure manometer	MKS	627D11TDC1B
Static pressure manomenter	MKS	627D.1TDD1B
Pitot pressure manometer	MKS	122BA-00010AB
Control unit for the generating and static pressure manometers	MKS	PR 4000B
Control unit for the Pitot pressure manometer	MKS	PDR-C-2C

Comments/Description

Heat-resistant (100°C). Length 3,5 m x Width 47 mm
RS Pro 1L 3D printing acetone
Temperature range -54°C to 343°C intermittent; resists auto and shop fluids.

Used in applications at temperatures as low as -269°C (-452°F) and as high as 260°C (500°F). High dielectric strength. Silicon adhesive protection leaves no residue.

Beveled flat plate used for the experiments.
Hollow diamond drill of diameter 2 mm for the Holes 1 & 2.
K-type thermocouple of a range from -50°C to 100°C.
DC Power supply delivering voltage from -1kV to -30 kV.
4 controllable axis servo or step by step.

The PI-MAX is a high performance intensified camera system with a 1024x1024 pixels-array featuring a spectroscopy format CCD. It is fiber optically coupled to a Gen II filmless intensifiers.

QWIP technology represents the longwave focal plane array (FPA) of 320 × 240 pixels. With its outstanding image stability and uniformity, the SC 3000 is ideal for applications where precision temperature measurements from -20 to 1500°C and high sensitivity are required.

Range of 10 Torr. 0,12 % lecture.
Range of 0,1 Torr. 0,15 % lecture.
Range of 10 Torr. 0,5 % lecture.
The PR4000 is available as single or dual channel power supply, readout and control unit. 2 trip limits and 2 relays, can be combined and configured in a wide variety of functions and combinations.
The MKS Type PDR-C-1C and PDR-C-2C are power supply and digital readouts which are packaged in standard half-rack mount units. The PDR-C-2C is designed to provide power for, and accept the outputs from two pressure sensors. The power supply for both the -1C and -2C is capable of providing ±15 VDC at up to 600 mA.

1 Alewife Center #200
Cambridge, MA 02140
tel. 617.945.9051
www.jove.com

ARTICLE AND VIDEO LICENSE AGREEMENT

Title of Article: Plasma actuators in rarefied super/hypersonic flows: experimental works to enhance spacecraft control and deceleration during atmospheric entries.

Author(s): Sandra COUMAR and Viviana LAGO

Item 1 (check one box): The Author elects to have the Materials be made available (as described at http://www.jove.com/author) via: [X] Standard Access [ ] Open Access

Item 2 (check one box):

[X] The Author is NOT a United States government employee.

[ ] The Author is a United States government employee and the Materials were prepared in the course of his or her duties as a United States government employee.

[ ] The Author is a United States government employee but the Materials were NOT prepared in the course of his or her duties as a United States government employee.

ARTICLE AND VIDEO LICENSE AGREEMENT

1. Defined Terms. As used in this Article and Video License Agreement, the following terms shall have the following meanings: "**Agreement**" means this Article and Video License Agreement; "**Article**" means the article specified on the last page of this Agreement, including any associated materials such as texts, figures, tables, artwork, abstracts, or summaries contained therein; "**Author**" means the author who is a signatory to this Agreement; "**Collective Work**" means a work, such as a periodical issue, anthology or encyclopedia, in which the Materials in their entirety in unmodified form, along with a number of other contributions, constituting separate and independent works in themselves, are assembled into a collective whole; "**CRC License**" means the Creative Commons Attribution-Non Commercial-No Derivs 3.0 Unported Agreement, the terms and conditions of which can be found at: http://creativecommons.org/licenses/by-nc-nd/3.0/legalcode; "**Derivative Work**" means a work based upon the Materials or upon the Materials and other pre-existing works, such as a translation, musical arrangement, dramatization, fictionalization, motion picture version, sound recording, art reproduction, abridgment, condensation, or any other form in which the Materials may be recast, transformed, or adapted; "**Institution**" means the institution, listed on the last page of this Agreement, by which the Author was employed at the time of the creation of the Materials; "**JoVE**" means MyJove Corporation, a Massachusetts corporation and the publisher of *The Journal of Visualized Experiments;* "**Materials**" means the Article and / or the Video; "**Parties**" means the Author and JoVE; "**Video**" means any video(s) made by the Author, alone or in conjunction with any other parties, or by JoVE or its affiliates or agents, individually or in collaboration with the Author or any other parties, incorporating all or any portion of the Article, and in which the Author may or may not appear.

2. Background. The Author, who is the author of the Article, in order to ensure the dissemination and protection of the Article, desires to have the JoVE publish the Article and create and transmit videos based on the Article. In furtherance of such goals, the Parties desire to memorialize in this Agreement the respective rights of each Party in and to the Article and the Video.

3. Grant of Rights in Article. In consideration of JoVE agreeing to publish the Article, the Author hereby grants to JoVE, subject to **Sections 4** and **7** below, the exclusive, royalty-free, perpetual (for the full term of copyright in the Article, including any extensions thereto) license (a) to publish, reproduce, distribute, display and store the Article in all forms, formats and media whether now known or hereafter developed (including without limitation in print, digital and electronic form) throughout the world, (b) to translate the Article into other languages, create adaptations, summaries or extracts of the Article or other Derivative Works (including, without limitation, the Video) or Collective Works based on all or any portion of the Article and exercise all of the rights set forth in (a) above in such translations, adaptations, summaries, extracts, Derivative Works or Collective Works and (c) to license others to do any or all of the above. The foregoing rights may be exercised in all media and formats, whether now known or hereafter devised, and include the right to make such modifications as are technically necessary to exercise the rights in other media and formats. If the "Open Access" box has been checked in **Item 1** above, JoVE and the Author hereby grant to the public all such rights in the Article as provided in, but subject to all limitations and requirements set forth in, the CRC License.

4. Retention of Rights in Article. Notwithstanding the exclusive license granted to JoVE in **Section 3** above, the Author shall, with respect to the Article, retain the non-exclusive right to use all or part of the Article for the non-commercial purpose of giving lectures, presentations or teaching classes, and to post a copy of the Article on the Institution's website or the Author's personal website, in each case provided that a link to the Article on the JoVE website is provided and notice of JoVE's copyright in the Article is included. All non-copyright intellectual property rights in and to the Article, such as patent rights, shall remain with the Author.

5. Grant of Rights in Video – Standard Access. This **Section 5** applies if the "Standard Access" box has been checked in **Item 1** above or if no box has been checked in **Item 1** above. In consideration of JoVE agreeing to produce, display or otherwise assist with the Video, the Author hereby acknowledges and agrees that, Subject to **Section 7** below, JoVE is and shall be the sole and exclusive owner of all rights of any nature, including, without limitation, all copyrights, in and to the Video. To the extent that, by law, the Author is deemed, now or at any time in the future, to have any rights of any nature in or to the Video, the Author hereby disclaims all such rights and transfers all such rights to JoVE.

6. Grant of Rights in Video – Open Access. This **Section 6** applies only if the "Open Access" box has been checked in **Item 1** above. In consideration of JoVE agreeing to produce, display or otherwise assist with the Video, the Author hereby grants to JoVE, subject to **Section 7** below, the exclusive, royalty-free, perpetual (for the full term of copyright in the Article, including any extensions thereto) license (a) to publish, reproduce, distribute, display and store the Video in all forms, formats and media whether now known or hereafter developed (including without limitation in print, digital and electronic form) throughout the world, (b) to translate the Video into other languages, create adaptations, summaries or extracts of the Video or other Derivative Works or Collective Works based on all or any portion of the Video and exercise all of the rights set forth in (a) above in such translations, adaptations, summaries, extracts, Derivative Works or Collective Works and (c) to license others to do any or all of the above. The foregoing rights may be exercised in all media and formats, whether now known or hereafter devised, and include the right to make such modifications as are technically necessary to exercise the rights in other media and formats. For any Video to which this Section 6 is applicable, JoVE and the Author hereby grant to the public all such rights in the Video as provided in, but subject to all limitations and requirements set forth in, the CRC License.

7. Government Employees. If the Author is a United States government employee and the Article was prepared in the course of his or her duties as a United States government employee, as indicated in **Item 2** above, and any of the licenses or grants granted by the Author hereunder exceed the scope of the 17 U.S.C. 403, then the rights granted hereunder shall be limited to the maximum rights permitted under such statute. In such case, all provisions contained herein that are not in conflict with such statute shall remain in full force and effect, and all provisions contained herein that do so conflict shall be deemed to be amended so as to provide to JoVE the maximum rights permissible within such statute.

8. Likeness, Privacy, Personality. The Author hereby grants JoVE the right to use the Author's name, voice, likeness, picture, photograph, image, biography and performance in any way, commercial or otherwise, in connection with the Materials and the sale, promotion and distribution thereof. The Author hereby waives any and all rights he or she may have, relating to his or her appearance in the Video or otherwise relating to the Materials, under all applicable privacy, likeness, personality or similar laws.

9. Author Warranties. The Author represents and warrants that the Article is original, that it has not been published, that the copyright interest is owned by the Author (or, if more than one author is listed at the beginning of this Agreement, by such authors collectively) and has not been assigned, licensed, or otherwise transferred to any other party. The Author represents and warrants that the author(s) listed at the top of this Agreement are the only authors of the Materials. If more than one author is listed at the top of this Agreement and if any such author has not entered into a separate Article and Video License Agreement with JoVE relating to the Materials, the Author represents and warrants that the Author has been authorized by each of the other such authors to execute this Agreement on his or her behalf and to bind him or her with respect to the terms of this Agreement as if each of them had been a party hereto as an Author. The Author warrants that the use, reproduction, distribution, public or private performance or display, and/or modification of all or any portion of the Materials does not and will not violate, infringe and/or misappropriate the patent, trademark, intellectual property or other rights of any third party. The Author represents and warrants that it has and will continue to comply with all government, institutional and other regulations, including, without limitation all institutional, laboratory, hospital, ethical, human and animal treatment, privacy, and all other rules, regulations, laws, procedures or guidelines, applicable to the Materials, and that all research involving human and animal subjects has been approved by the Author's relevant institutional review board.

10. JoVE Discretion. If the Author requests the assistance of JoVE in producing the Video in the Author's facility, the Author shall ensure that the presence of JoVE employees, agents or independent contractors is in accordance with the relevant regulations of the Author's institution. If more than one author is listed at the beginning of this Agreement, JoVE may, in its sole discretion, elect not take any action with respect to the Article until such time as it has received complete, executed Article and Video License Agreements from each such author. JoVE reserves the right, in its absolute and sole discretion and without giving any reason therefore, to accept or decline any work submitted to JoVE. JoVE and its employees, agents and independent contractors shall have

full, unfettered access to the facilities of the Author or of the Author's institution as necessary to make the Video, whether actually published or not. JoVE has sole discretion as to the method of making and publishing the Materials, including, without limitation, to all decisions regarding editing, lighting, filming, timing of publication, if any, length, quality, content and the like.

11. Indemnification. The Author agrees to indemnify JoVE and/or its successors and assigns from and against any and all claims, costs, and expenses, including attorney's fees, arising out of any breach of any warranty or other representations contained herein. The Author further agrees to indemnify and hold harmless JoVE from and against any and all claims, costs, and expenses, including attorney's fees, resulting from the breach by the Author of any representation or warranty contained herein or from allegations or instances of violation of intellectual property rights, damage to the Author's or the Author's institution's facilities, fraud, libel, defamation, research, equipment, experiments, property damage, personal injury, violations of institutional, laboratory, hospital, ethical, human and animal treatment, privacy or other rules, regulations, laws, procedures or guidelines, liabilities and other losses or damages related in any way to the submission of work to JoVE, making of videos by JoVE, or publication in *JoVE* or elsewhere by JoVE. The Author shall be responsible for, and shall hold JoVE harmless from, damages caused by lack of sterilization, lack of cleanliness or by contamination due to the making of a video by JoVE its employees, agents or independent contractors. All sterilization, cleanliness or decontamination procedures shall be solely the responsibility of the Author and shall be undertaken at the Author's expense. All indemnifications provided herein shall include JoVE's attorney's fees and costs related to said losses or damages. Such indemnification and holding harmless shall include such losses or damages incurred by, or in connection with, acts or omissions of JoVE, its employees, agents or independent contractors.

12. Fees. To cover the cost incurred for publication, JoVE must receive payment before production and publication the Materials. Payment is due in 21 days of invoice. Should the Materials not be published due to an editorial or production decision, these funds will be returned to the Author. Withdrawal by the Author of any submitted Materials after final peer review approval will result in a US$1,200 fee to cover pre-production expenses incurred by JoVE. If payment is not received by the completion of filming, production and publication of the Materials will be suspended until payment is received.

13. Transfer, Governing Law. This Agreement may be assigned by JoVE and shall inure to the benefits of any of JoVE's successors and assignees. This Agreement shall be governed and construed by the internal laws of the Commonwealth of Massachusetts without giving effect to any conflict of law provision thereunder. This Agreement may be executed in counterparts, each of which shall be deemed an original, but all of which together shall be deemed to me one and the same agreement. A signed copy of this Agreement delivered by facsimile, e-mail or other means of electronic transmission shall be deemed to have the same legal effect as delivery of an original signed copy of this Agreement.

A signed copy of this document must be sent with all new submissions. Only one Agreement required per submission.

CORRESPONDING AUTHOR:

Name:	Sandra COUMAR
Department:	Laboratoire ICARE
Institution:	CNRS
Article Title:	Plasma actuators in rarefied super/hypersonic flows: experimental works to enhance spacecraft control and deceleration during atmospheric entries.
Signature:	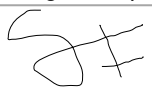
Date:	11 May 2017

Please submit a signed and dated copy of this license by one of the following three methods:

1) Upload a scanned copy of the document as a pfd on the JoVE submission site;
2) Fax the document to +1.866.381.2236;
3) Mail the document to JoVE / Attn: JoVE Editorial / 1 Alewife Center #200 / Cambridge, MA 02139

For questions, please email submissions@jove.com or call +1.617.945.9051

Responses to reviewers

Manuscript ID: JoVE56602

submitted to

Journal of Visualized Experiments

S.Coumar and V. Lago

July 12, 2017

Letter for editor

Dear Dr. Nam Nguyen,

Please find attached a revised version of our manuscript "*Plasma actuators in rarefied super / hypersonic flows: experimental works to enhance spacecraft control and deceleration during atmospheric entries.*".

The authors would like to thank the reviewers for their time and their valuable comments. In the following pages are our point-by-point responses to the comments of the reviewers as well as your own comments. The indicated page and line numbers correspond to the revised manuscript.

We use the following color code:

- text: text modified or removed from the submitted version of our script
- text: text added in the revised version of our script

We hope that the revisions in the manuscript and our accompanying responses will be sufficient to make our manuscript suitable for publication in JOVE.

Yours sincerely,

The Authors

Editor comments

Editor's comment A: Please take this opportunity to thoroughly proofread the manuscript to ensure that there are no spelling or grammar issues. The JoVE editor will not copy-edit your manuscript and any errors in the submitted revision may be present in the published version.

Answer A: We read carefully the manuscript and corrected the spelling or grammar issues.

Editor's comment B: Please define all abbreviations before use.

Answer B: The abbreviations found on lines 36, 83, 150, 213, 222, 366 and 374 were not defined. Therefore, their definitions are put into brackets and are written close to them.

Editor's comment C: Please use focused images of uniform size/resolution (at least 300 dpi).

Answer C: We followed the recommendation of the Editor and changed the resolution of our figures to 300 dpi.

Editor's comment D: Please revise the table of the essential supplies, reagents, and equipment. The table should include the name, company, and catalog number of all relevant materials in separate columns in an xls/xlsx file.

Answer D: We filled the missing informations to complete the table.

Editor's comment E: Unfortunately, there are a few sections of the manuscript that show significant overlap with previously published work. Though there may be a limited number of ways to describe a technique, please use original language throughout the manuscript. Please see lines: 55-57, 62-67, 316-326, 339-342, 344-349, 355-372, 377-380, 456-461, 474-476.

Answer E: As it was highlighted by the Editor, even if the works are different troughout our papers, the subject remains the deceleration of reentry vehicles and thus, it is inevitable to find some similar parts. Furethermore, material and facilities used during experimental works can hardly be described in other ways. However, taking into account the Editor comment, we modified the underlined parts.

L.55-57 At typical reentry speeds, vehicles are subjected to extreme conditions and mission planning must balance three requirements: deceleration, heating management, and accuracy of the vehicle localization and velocity when landing.

to

L.55-57 The very high speeds reached by the vehicle during reentries induce extreme conditions and at least three requirements have to be fulfilled with care: deceleration, heating management, and accuracy of the vehicle localization and velocity when landing.

L.62-67 On this purpose, it has been demonstrated that plasma actuators offer the possibility to modify the shock wave shape around the vehicle and thus the drag coefficient. This could potentially reduce locally the heat flux. Compared to traditional flow control methods, plasma actuators present several advantages like their fast response time, their low weight and size and the relatively low energy consumption, offering promising applications for flight control systems at high velocities.

to

L.62-67 The plasma actuator induces an increase in the drag force on the model surface and thus, reduce the local heat flux. This effect is obtained by the modification of the shock wave shape that arises when the plasma actuator is on. Therefore, plasma actuators can be classified in the flow control mehods and compared to traditional ones, their key strengths are their low weight and size and the relatively low energy consumption. So many assets that rank them as promising applications for flight control systems at high velocities.

L.316-326 This unique facility in Europe is able to reproduce a wide range of the reentry vehicles flight corridors from 140 km to 67 km of altitude. A schematic view of the facility is presented in Figure 1. It consists of three main parts: the settling chamber with a diameter of 1.3 m and a length of 2.0 m, the test chamber with a diameter of 2.3 m and a length of 5.0 m and a third chamber in which a diffuser is installed. The diffuser is connected to the pumping group through a vacuum gate. A powerful pumping group with 2 primary pumps, 2 intermediary Roots blowers and 12 Roots blowers ensures the low density flow conditions in continuous operating mode. Depending on the desired rarefaction level, the number of pumps used can be varied. When supplied with different nozzles, the wind tunnel generates subsonic, supersonic and hypersonic flows from Mach 0.8 to Mach 21, and covers a large range of Reynolds numbers from 102 up to 105 for a reference length of 100 mm (corresponding to the length of the flat plate used as model).

to

L.316-326 The MARHy wind tunnel can be equipped with a wide range of nozzles allowing the generation of subsonic, supersonic and hypersonic flows from Mach 0.8 to Mach 21, and covers a large range of Reynolds numbers from 102 up to 105 for a reference length of 100 mm (corresponding to the length of the flat plate used as model. These flow condition reconstitute a most of the reentry vehicles flight corridors from 140 km to 67 km of altitude making this facility unique in Europe. Figure 1 exhibits the facility which can be divided in three parts: the settling chamber with a diameter of 1.3 m and a length of 2.0 m, the test chamber with a diameter of 2.3 m and a length of 5.0 m and a third chamber in which a diffuser is installed and connects the pumping group to the facility through a vacuum gate. The pumping group is composed of 2 primary pumps, 2 intermediary Roots blowers and 12 Roots blowers. Its performances makes it able to ensure low density flow conditions continuously.

L.339-342 The models are made of quartz in order to withstand the high surface temperatures reached when using the plasma actuator. The flat plates are placed in the test section, downstream the nozzle exit as sketched on Figure 3. The plasma actuator is composed of two aluminum electrodes, 50 mm-wide, 35 mm-long and 80 mm-thick.

to

L.339-342 The plasma actuator induce very high wall temperatures thus, models must be manufactured in a heat-resistant material. The flat plates are made of quartz and the position of the model in the test chamber is sketched on Figure 3. The two electrodes setting the plasma actuator are manufactured in aluminium and designed with the dimensions: 50 mm-wide, 35 mm-long and 80 μm-thick.

L.344-349 The electrodes size is calculated in order to keep the ratio of the active electrode surface on the model surface constant and equal to 35%. The first electrode, called the active electrode or the cathode, is set at the leading edge of the plate, and is connected to a high voltage DC power supply (Spellman, SR15PN6) through a current limiting resistor (Rs = 10.6 $k\Omega$), while the second electrode is grounded. The high voltage Vs is fixed with the power supply, which delivers the discharge current IHV.

to

L.344-349 Depending on the nozzle, the core of the generated flow will have specific dimensions and the models must be adapted to these cores. Therefore, the width of the model strongly depend of the studied flow. Howeer, in order to maintain a certain coherence, the ratio of the active electrode on the surface of the model is kept at 35%. The electrode located the closest to the leading edge is defined as the cathode or active electrode and is connected to a high voltage DC power supply (Spellman, SR15PN6) through a current limiting resistor (Rs = 10.6 $k\Omega$), while the second electrode is grounded. The DC power supply is voltage-regulated and delivers the discharge current IHV corresponding to the chosen Vs voltage.

L.355-372 For this purpose these pressures are measured with absolute capacitive sensors (MKS, 600 series Baratron) which scales are adapted to the range of the measurement values. The manometers are connected to a MKS control unit (PR 4000B) with a 12-bit resolution. The pressure in the flow above the plate is measured with a Pitot probe connected to a MKS Baratron capacitance manometer connected to a MKS control unit (PDR-C-2C). A 3-axis traversing system, controlled by a computer, ensures the displacement of the Pitot probe with a step resolution on each axis of 0.1 mm 0.02 mm on each position. The Pitot probe is made of glass in order to avoid electrical interactions with the discharge. The Pitot tube consists of a flat-ended cylinder with an external diameter of D = 6 mm and an internal diameter of d = 4 mm. The manometers positions are spotlighted on Figure 4. The flow around the flat plate is visualized with a PI-MAX Gen-II iCCD camera (1024 x 1024-pixel array) equipped with a VUV (Visible-UltraViolet) objective lens (94 mm, f =4.1). The light is collected through a fluorine window located in the wall of the test section chamber as showed on Figure 4. The evolution of the surface temperature of the flat plate is monitored with an infrared thermography device. The IR device is used to measure the flat plate surface temperature during the experiments. The IR camera (FLIR ThermaCAM SC 3000) is placed on the top of the wind tunnel (see Figure 4) and focuses on the entire surface of the flat plate through a fluorine window compatible with the IR wavelength range of the camera.

to

L.355-372 Capacitive sensors (MKS, 600 series Baratron) are used to measure the stagnation pressure Po and the static pressure P1 and the pressure above the flat plate when combined to a Pitot probe. The Pitot tube is a flat-ended tube made of glass to avoid electrical interactions with the discharge. Its dimensions are D = 6 mm for the external diameter and d = 4 mm for the internal one. The pressure mapping above the plate is ensured with a 3-axis traversing system, controlled by a computer. The step resolution of the Pitot probe on each axis is of 0.1 mm 0.02 mm for each position. A MKS control unit (PR 4000B) with a 12-bit resolution is linked to the manometers associated to Po and P1, whereas a MKS control unit (PDR-C-2C) is used for the Pitot probe acquisition. The 10V output of each MKS unit control is read by an acquisition card storing the pressures values during experiments. Figure 4 exhibits the manometers positions. A PI-MAX Gen-II iCCD camera (1024 x 1024-pixel array) equipped with a VUV (Visible-UltraViolet) objective lens (94 mm, f =4.1) is used for the flow visualisation. As it is shown on figure 4, the iCCD camera is placed perpendicularly to the flow axis and collects the light through a fluorine window located in the wall of the test section chamber. An infra-red camera (FLIR ThermaCAM SC 3000) is placed on the top of the wind tunnel focusing on the model through a fluorine window compatible with the IR wavelength range of the camera. This device follows and records the live evolution of the surface temperature of the model.

L.377-380 The flow field around the flat plate is first investigated without any plasma discharge, corresponding to the study of the natural flow (namely, the baseline). The nominal operating conditions of the flow field remain those detailed in Table 1. Images obtained with the iCCD camera of the baseline flow field are presented on Figure 5.

to

L.377-380 First, the baseline is defined. It corresponds to the flow behavior around the model without any actuation. The flow conditions were detailed in Table 1. Figure 5 presents the images of the baseline recorded with the iCCD camera.

L.456-461 The temperature distributions with the infra-red camera measurements along the longitudinal axis of the plate are plotted on Figure 10. It is clear that the model surface is heated by the plasma actuator. Indeed, even if the heat source is strictly located at the cathode, the flat plate is entirely heated due to the quartz thermal conductivity. However, as the electric field varies along the X-direction, the longitudinal distribution of the surface temperature is not constant. The highest temperatures are measured close to the leading edge (i.e., above the cathode) where the electric field is the strongest and the lowest temperatures measured at the trailing edge of the flat plate.

to

L.456-461 Figure 10 displays the temperature distributions along the longitudinal axis of the model. The plots show that the plasma actuator heats the surface of the model although the distribution is non uniform and increases towards the cathode. The non-uniformity is induced by the variation of the electric field along the X-direction and this electric field is maximum close to the leading edge of the flat plate.

L.474-476 However, as it was demonstrated in previous studies, the surface heating accounted only for 50% in the shock wave angle increase; thus, it can be assumed that the percentage would be even lower in the current case with the Mach 4 flow. Consequently the purely ionization effect is predominant in this case.

to

L.474-476 However, one can assume that the ionization effect would be even higher with the Mach 4 flow than the 50% estimated in previous studies. Therefore, the influence of the surface heating on the shock wave modification will be even more negligible.

Editor's comment F: Please remove the embedded figure(s) from the manuscript. All figures should be uploaded separately to your Editorial Manager account. Each figure must be accompanied by a title and a description after the Representative Results of the manuscript text.

Answer F: We removed the embedded figures and let the linked titles.

Editor's comment G: Please remove the embedded Table from the manuscript. All tables should be uploaded separately to your Editorial Manager account in the form of an .xls or .xlsx file. Each table must be accompanied by a title and a description after the Representative Results of the manuscript text.

Answer G: We removed the embedded table and let the linked title.

Editor's comment H: Please add more details to your protocol steps. Please ensure you answer the how question, i.e., how is the step performed? Alternatively, add references to published material specifying how to perform the protocol action.

Answer H: We read with a great care the Protocol and gave any additional information that could help the Reader to understand it. When it was needed, we added references, for instance for the Pitot tube size determination and to calculate the orifice corrections.

Editor's comment I: What type of drills are used?

Answer I: In order to give the specifications of the used drill, we add this line:

L.138 For this purpose, use a diamond hollow drill of 2 mm diameter.

Editor's comment J: B2.4: What grit sandpaper?

Answer J: The grit of the sandpaper is added as follows:

Scrape the surface that will welcome the plasma actuator with sandpaper.

to

Scrape the surface that will welcome the plasma actuator with 240 grade sandpaper.

Editor's comment K: B2.5: What percentage alcohol?

Answer K: The percentage of alcohol is added as follows:

Clean with great care the model with rubbing alcohol and make sure there is no particle left on the surface.

to

Clean with great care the model with a 60 % rubbing alcohol and make sure there is no particle left on the surface.

Editor's comment L: B3.1: How thin?

Answer L: The thickness of the glue layer is added as follows:

Spread evenly a thin layer of RTV (Room Temperature Vulcanizing) glue or any other type of glue that can endure high-temperature going to at least 600C on the back of the electrodes.

to

Spread evenly a 200 micrometers thin layer of RTV (Room Temperature Vulcanizing) glue or any other type of glue that can endure high-temperature going to at least 600C on the back of the electrodes.

Editor's comment M: Please revise the text to avoid the use of any personal pronouns (e.g., "we", "you", "our" etc.).

Answer M: We removed all the personal pronouns and thus, modified the incriminated parts.

Editor's comment N: Please highlight 2.75 pages or less of the Protocol (including headings and spacing) that identifies the essential steps of the protocol for the video, i.e., the steps that should be visualized to tell the most cohesive story of the Protocol. The highlighted steps should form a cohesive narrative with a logical flow from one highlighted step to the next. Remember that non-highlighted Protocol steps will remain in the manuscript, and therefore will still be available to the reader.
Please ensure that the highlighted steps form a cohesive narrative with a logical flow from one highlighted step to the next. Please highlight complete sentences (not parts of sentences). Please ensure that the highlighted part of the step includes at least one action that is written in imperative tense.

Answer N: We highlighted the essential steps of our Protocol that should be filmed. The highlighted steps form a cohesive narrative with a logical flow and gather the main steps of our protocol to undertake experiments.

Editor's comment O: As we are a methods journal, please revise the Discussion to explicitly cover the following in detail in 3-6 paragraphs with citations:

- Critical steps within the protocol
- Any modifications and troubleshooting of the technique
- Any limitations of the technique
- The significance with respect to existing methods
- Any future applications of the technique

Answer O: Following your advice, we completely restructured the Discussion part with adding parts on the Protocol critical steps, the plasma actuators limitations and its future applications. The comparison of the plasma actuators with other existing methods was already analyzed in the Introduction part so we did not reiterate it in this part. We insert below the former Discussion part and then the modified one.

The temperature distributions with the infra-red camera measurements along the longitudinal axis of the plate are plotted on Figure 10. It is clear that the model surface is heated by the plasma actuator. Indeed, even if the heat source is strictly located at the cathode, the flat plate is entirely heated due to the quartz thermal conductivity. However, as the electric field varies along the X-direction, the longitudinal distribution of the surface temperature is not constant. The highest temperatures are measured close to the leading edge (i.e., above the cathode) where the electric field is the strongest and the lowest temperatures measured at the trailing edge of the flat plate. For a given value of IHV, the plasma discharge without the Mach 4 flow (static pressure set to 8 Pa) induced a similar heating of the flat plate (not shown here), since the temperature distribution is similar both in value and shape. This result confirms that heating of the flat plate surface is mainly related to a discharge effect and not influenced by the interaction between the Mach 4 air flow and the flat plate surface. The thermal equilibrium of the cathode temperature is reached after 1520 min; meaning that the magnitude order of the surface heating time scale is few tenth of minutes. It can be seen that the increase in surface temperature with the power discharge is not impactful. The same behavior was observed with the Mach 2 flow but with higher temperatures gradients. In rarefied flow regimes, one of the main effects expected to be responsible for the shock wave modification is the heating of the model surface. However, as it was demonstrated in previous studies, the surface heating accounted only for 50 % in the shock wave angle increase; thus, it can be assumed that the percentage would be even lower in the current case with the Mach 4 flow. Consequently the purely ionization effect is predominant in this case.

The surface heating induces a displacement effect: the flow viscosity above the heater is modified, inducing an increase in the laminar boundary layer thickness, and, consequently, the shock wave is shifted outward the flat plate surface (i.e., ? increases). This effect can be observed more clearly on Figure 11 where four Pitot pressure profiles are presented: one corresponds to the baseline, and the others correspond to the cases when different discharge powers are supplied. On the shape of the profiles measured at X = 50 mm, the knee geometry is found at a higher position on the Z-axis, meaning that the thickness of the boundary layer has increased and therefore, the shock wave angle too.

To demonstrate the efficiency of plasma actuators in the context of atmospheric entries, an estimation of the aerodynamic forces over the model has been made. The discussion is focused on the drag force because during atmospheric re-entries, it is directly linked with deceleration. In terms of relative variation, for a maximum wall temperature increase of almost 50%, the drag coefficient CD is modified by +13.0% for the plasma actuation. As the main goal is to decrease the speed of a spaceship, in view to decrease the total heat, it is interesting to study the effect of the drag diminution on the heat flux over the spaceship. For the re-entry of a space shuttle in the mold of Columbia, an increase of 13% of the total drag, as estimated in this paper, corresponds to a decrease in the vehicle speed of about 7% and of about 26% of the heat flow because the heat flow is proportional to the power 3.15 of speed. Taking into account that the mass of the heat protection in the shuttle is of 9575 kg and that the decrease of the heat flow is proportional to the mass protection, 2.5 tons of the Shuttle mass could be saved with the plasma actuator.

to

The described experimental protocol presents some critical steps. The first point concerns the repeatability of experiments because for a given experimental condition, several experimental campaigns are needed. Indeed, in order to have a complete physical analysis, different diagnostics are used that cannot be applied simultaneously. This implies that the experimental set-up (model, electrodes size and shape, position of the model in the test chamber, ?) must be rigorously the same throughout the experiments. Even slight differences can induce different discharges conditions modifying the plasma actuator effects and thus, the results will not anymore be comparable. The other point directly impacts the shock wave angle measurements. Indeed, each iCCD Image needs a specific post-processing, and thus, are analyzed manually. Therefore, it is essential to apply a well-run method for every post-processing. Furthermore, the shock wave angles are also determined from Pitot probe profiles and compared to angles detected with the iCCD images to strengthen the measurements.

The technique of plasma actuators itself presents also some issues. The main limitation of such actuators is due to the flow conditions, especially the pressure and thus, the altitude of the atmospheric re-entry spacecraft. Plasma actuators have to be characterized in different flow regimes in terms of speed and pressure to extrapolate their behavior in real cases. For this purpose, it is necessary to deeply understand the plasma physics and its coupling with the flow to overcome the challenges. Some authors incriminated thermal effects (bulk and surface) for the shock waves modifications in supersonic conditions. Shin et al. investigated thermal effects with two distinct discharge modes, where an increase in the gas temperature was observed nevertheless no clear evidence of plasma effects on the flow was identified.

The present paper shows that other physical aspects due to the discharge, than thermal ones, have to be taken into account to explain the flow modifications. Figure 16 displays the temperature distributions along the longitudinal axis of the model. The plots show that the plasma actuator heats the surface of the model although the distribution is non uniform and increases towards the cathode. The non-uniformity is induced by the variation of the electric field along the X-direction and this electric field is maximum close to the leading edge of the flat plate. For a given value of the discharge current IHV, the plasma discharge without the Mach 4 flow (static pressure set to 8 Pa) induced a similar heating of the flat plate, with a temperature distribution similar (both in value and shape) to the temperature distribution when the Mach 4 flow is operating. This result confirms that the heating of the flat plate surface is mainly related to a discharge effect and not influenced by the interaction between the Mach 4 air flow and the flat plate surface. Moreover, the surface heating induces a displacement effect: the flow viscosity above the heater is modified, inducing an increase in the laminar boundary layer thickness, and consequently, the shock wave is shifted outward the flat plate surface (i.e., the shock wave angle increases). This effect can be observed more clearly on Figure 17 where four Pitot pressure profiles are presented: one corresponds to the baseline, and the others correspond to the cases when different discharge powers are supplied. On the shape of the profiles measured at X = 50 mm, the knee geometry is found at a higher position on the Z-axis, meaning that the thickness of the boundary layer has increased and therefore, the shock wave angle too. Experiments carried out with a Mach 2 flow and a static pressure of 8 Pa, showed that the thermal effects accounted for only 50% in the shock wave angle increase and the remain 50% were due to ionization effects. For Mach 2 and Mach 4 flows, the surface temperature distributions are similar although the temperature gradients are higher with the Mach 2 flow. Therefore, one can assume that the ionization effect would be even greater with the Mach 4 flow than the 50 % estimated in previous studies, meaning that the influence of the surface heating on the shock wave modification will be even more negligible.

During atmospheric re-entries, atmospheric drag is used to slow down the vehicle, but the amount of energy to dissipate is enormous. The rate of energy dissipation is then estimated to be proportional to the cube of the vehicle speed, inducing very high temperatures on the spacecraft which may produce serious damages if the thermal protections are not sufficient. Optimal return trajectories are designed to obtain the minimum return cost defined as the sum of the mass propellant consumed by the space vehicle to de-orbit and the mass of thermal protections. However, reduction of thermal protections could be a way to decrease the cost of future missions. For this purpose, the idea is to increase the drag force in the aim of decelerating the vehicle and the use of plasma actuators could be an alternative method. In order to estimate the efficiency of plasma actuators in heat loads reduction, numerical simulations corresponding to our experimental conditions have been carried out to determine the aerodynamic drag forces induced by the discharge over the flat plate at Mach 2 and 8 Pa. The surface heating produced by the plasma discharge is numerically simulated reproducing the shock wave angle modifications observed experimentally. Results showed that the shock wave angles with only the surface heating are

Author's comment : Some reviewers advised to improve the overall English language of the paper. Taking this in consideration, we read it again with great care and corrected all the grammar mistakes and mispellings we could found.

Response to Reviewer #1

Manuscript Summary

N/A

Major Concerns

Very important for the scientific community.

Minor Concerns

Some more details on the limitations and possible challenges would have been beneficial. The step by step narrative can be enhanced with more figures.

Manuscript Summary

N/A

Author's comment 2: Taking into consideration the Reviewer's comment, we restructured the Discussion part and added there a paragraph about the limitations faced when using plasma actuators. We hope that this will satisfy the Reviewer. We also added nine more figures to the Protocol in the aim of making the reading easier. We insert below the former Discussion part and then the modified one and the extra figures.

The temperature distributions with the infra-red camera measurements along the longitudinal axis of the plate are plotted on Figure 10. It is clear that the model surface is heated by the plasma actuator. Indeed, even if the heat source is strictly located at the cathode, the flat plate is entirely heated due to the quartz thermal conductivity. However, as the electric field varies along the X-direction, the longitudinal distribution of the surface temperature is not constant. The highest temperatures are measured close to the leading edge (i.e., above the cathode) where the electric field is the strongest and the lowest temperatures measured at the trailing edge of the flat plate. For a given value of IHV, the plasma discharge without the Mach 4 flow (static pressure set to 8 Pa) induced a similar heating of the flat plate (not shown here), since the temperature distribution is similar both in value and shape. This result confirms that heating of the flat plate surface is mainly related to a discharge effect and not influenced by the interaction between the Mach 4 air flow and the flat plate surface. The thermal equilibrium of the cathode temperature is reached after 1520 min; meaning that the magnitude order of the surface heating time scale is few tenth of minutes. It can be seen that the increase in surface temperature with the power discharge is not impactful. The same behavior was observed with the Mach 2 flow but with higher temperatures gradients. In rarefied flow regimes, one of the main effects expected to be responsible for the shock wave modification is the heating of the model surface. However, as it was demonstrated in previous studies, the surface heating accounted only for 50 % in the shock wave angle increase; thus, it can be assumed that the percentage would be even lower in the current case with the Mach 4 flow. Consequently the purely ionization effect is predominant in this case.

The surface heating induces a displacement effect: the flow viscosity above the heater is modified, inducing an increase in the laminar boundary layer thickness, and, consequently, the shock wave is shifted outward the flat plate surface (i.e., ? increases). This effect can be observed more clearly on Figure 11 where four Pitot pressure profiles are presented: one corresponds to the baseline, and the others correspond to the cases when different discharge powers are supplied. On the shape of the profiles measured at X = 50 mm, the knee geometry is found at a higher position on the Z-axis, meaning that the thickness of the boundary layer has increased and therefore, the shock wave angle too.

To demonstrate the efficiency of plasma actuators in the context of atmospheric entries, an estimation of the aerodynamic forces over the model has been made. The discussion is focused on the drag force because during atmospheric re-entries, it is directly linked with deceleration. In terms of relative variation, for a maximum wall temperature increase of almost 50%, the drag coefficient CD is modified by +13.0% for the plasma actuation2. As the main goal is to decrease the speed of a spaceship, in view to decrease the total heat, it is interesting to study the effect of the drag diminution on the heat flux over the spaceship. For the re-entry of a space shuttle in the mold of Columbia, an increase of 13% of the total drag, as estimated in this paper, corresponds to a decrease in the vehicle speed of about 7% and of about 26% of the heat flow because the heat flow is proportional to the power 3.15 of speed. Taking into account that the mass of the heat protection in the shuttle is of 9575 kg and that the decrease of the heat flow is proportional to the mass protection21, 2.5 tons of the Shuttle mass could be saved with the plasma actuator.

to

The described experimental protocol presents some critical steps. The first point concerns the repeatability of experiments because for a given experimental condition, several experimental campaigns are needed. Indeed, in order to have a complete physical analysis, different diagnostics are used that cannot be applied simultaneously. This implies that the experimental set-up (model, electrodes size and shape, position of the model in the test chamber, ?) must be rigorously the same throughout the experiments. Even slight differences can induce different discharges conditions modifying the plasma actuator effects and thus, the results will not anymore be comparable. The other point directly impacts the shock wave angle measurements. Indeed, each iCCD Image needs a specific post-processing, and thus, are analyzed manually. Therefore, it is essential to apply a well-run method for every post-processing. Furthermore, the shock wave angles are also determined from Pitot probe profiles and compared to angles detected with the iCCD images to strengthen the measurements.

The technique of plasma actuators itself presents also some issues. The main limitation of such actuators is due to the flow conditions, especially the pressure and thus, the altitude of the atmospheric re-entry spacecraft. Plasma actuators have to be characterized in different flow regimes in terms of speed and pressure to extrapolate their behavior in real cases. For this purpose, it is necessary to deeply understand the plasma physics and its coupling with the flow to overcome the challenges. Some authors incriminated thermal effects (bulk and surface) for the shock waves modifications in supersonic conditions. Shin et al. investigated thermal effects with two distinct discharge modes, where an increase in the gas temperature was observed nevertheless no clear evidence of plasma effects on the flow was identified.

The present paper shows that other physical aspects due to the discharge, than thermal ones, have to be taken into account to explain the flow modifications. Figure 16 displays the temperature distributions along the longitudinal axis of the model. The plots show that the plasma actuator heats the surface of the model although the distribution is non uniform and increases towards the cathode. The non-uniformity is induced by the variation of the electric field along the X-direction and this electric field is maximum close to the leading edge of the flat plate. For a given value of the discharge current IHV, the plasma discharge without the Mach 4 flow (static pressure set to 8 Pa) induced a similar heating of the flat plate, with a temperature distribution similar (both in value and shape) to the temperature distribution when the Mach 4 flow is operating. This result confirms that the heating of the flat plate surface is mainly related to a discharge effect and not influenced by the interaction between the Mach 4 air flow and the flat plate surface. Moreover, the surface heating induces a displacement effect: the flow viscosity above the heater is modified, inducing an increase in the laminar boundary layer thickness, and consequently, the shock wave is shifted outward the flat plate surface (i.e., the shock wave angle increases). This effect can be observed more clearly on Figure 17 where four Pitot pressure profiles are presented: one corresponds to the baseline, and the others correspond to the cases when different discharge powers are supplied. On the shape of the profiles measured at X = 50 mm, the knee geometry is found at a higher position on the Z-axis, meaning that the thickness of the boundary layer has increased and therefore, the shock wave angle too. Experiments carried out with a Mach 2 flow and a static pressure of 8 Pa, showed that the thermal effects accounted for only 50% in the shock wave angle increase and the remain 50% were due to ionization effects. For Mach 2 and Mach 4 flows, the surface temperature distributions are similar although the temperature gradients are higher with the Mach 2 flow. Therefore, one can assume that the ionization effect would be even greater with the Mach 4 flow than the 50 % estimated in previous studies, meaning that the influence of the surface heating on the shock wave modification will be even more negligible.

During atmospheric re-entries, atmospheric drag is used to slow down the vehicle, but the amount of energy to dissipate is enormous. The rate of energy dissipation is then estimated to be proportional to the cube of the vehicle speed, inducing very high temperatures on the spacecraft which may produce serious damages if the thermal protections are not sufficient. Optimal return trajectories are designed to obtain the minimum return cost defined as the sum of the mass propellant consumed by the space vehicle to de-orbit and the mass of thermal protections. However, reduction of thermal protections could be a way to decrease the cost of future missions. For this purpose, the idea is to increase the drag force in the aim of decelerating the vehicle and the use of plasma actuators could be an alternative method. In order to estimate the efficiency of plasma actuators in heat loads reduction, numerical simulations corresponding to our experimental conditions have been carried out to determine the aerodynamic drag forces induced by the discharge over the flat plate at Mach 2 and 8 Pa. The surface heating produced by the plasma discharge is numerically simulated reproducing the shock wave angle modifications observed experimentally. Results showed that the shock wave angles with only the surface heating are

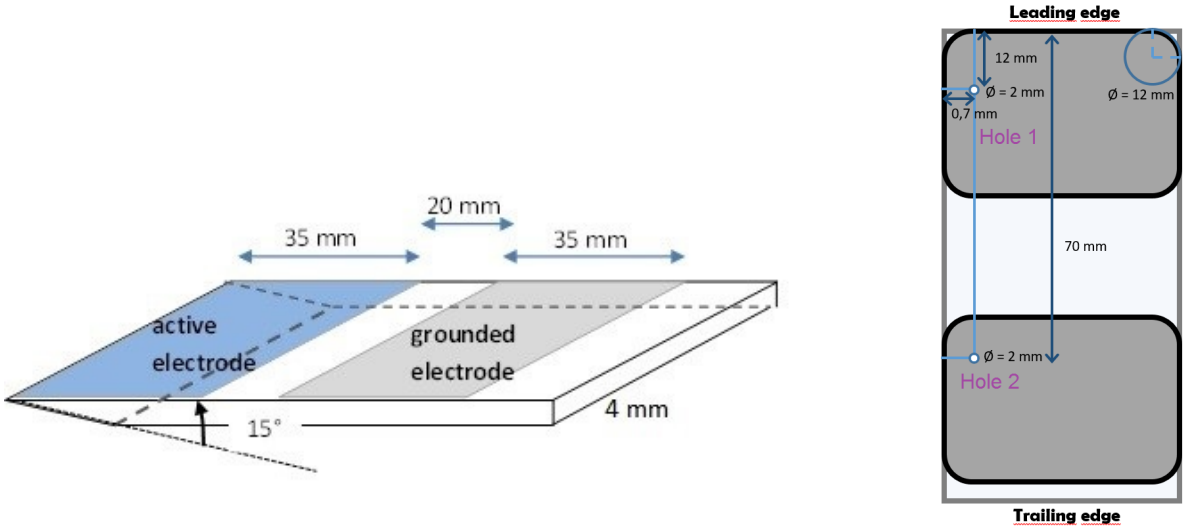

Figure 1 Figure 1 and Figure 2 of the Protocol part

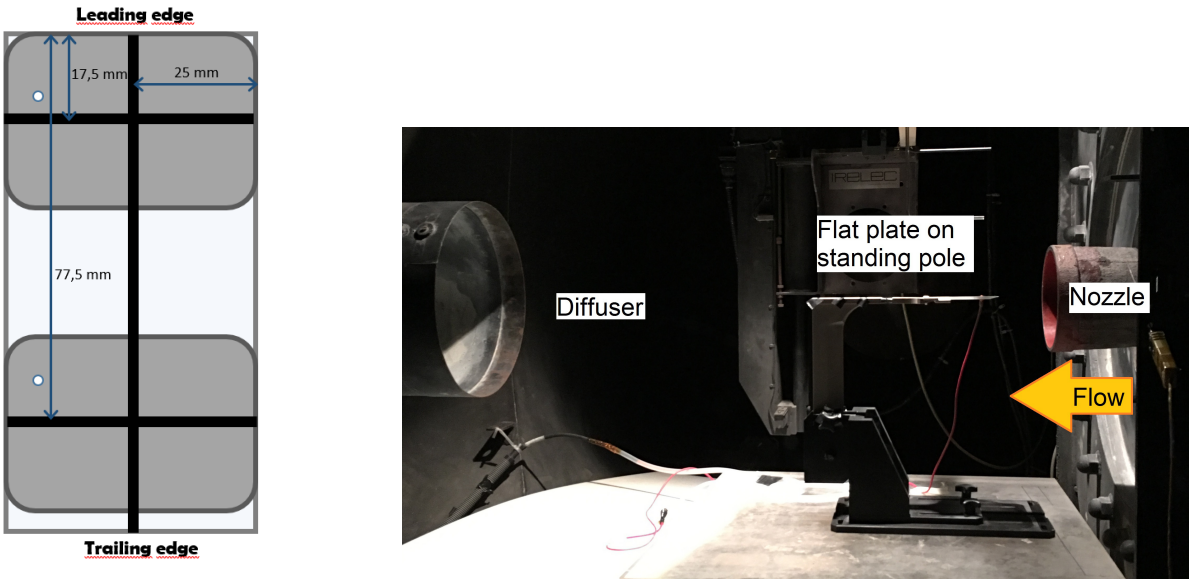

Figure 2 Figure 3 and Figure 4 of the Protocol part

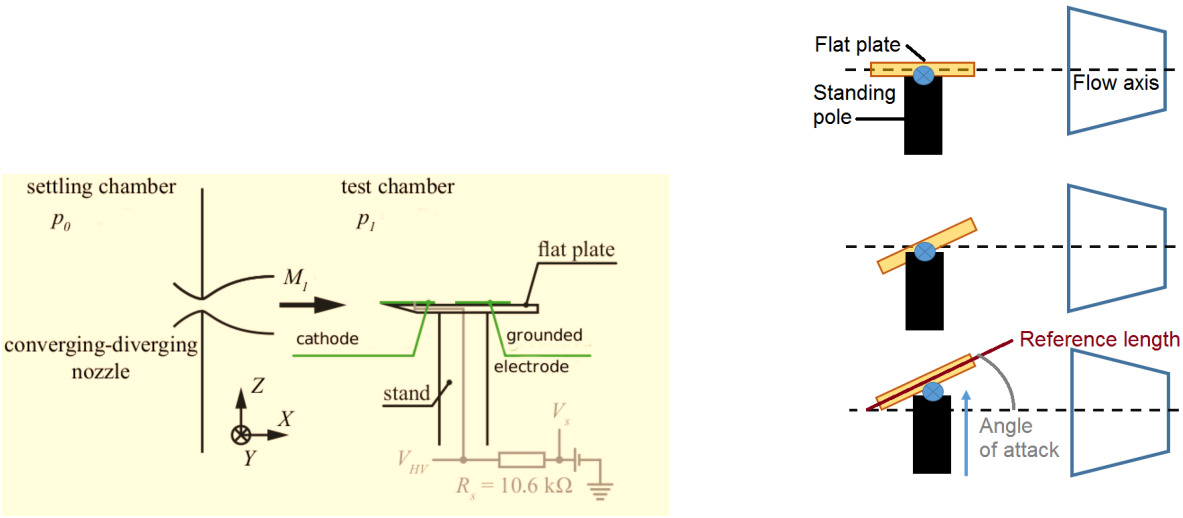

Figure 3 Figure 5 and Figure 6 of the Protocol part

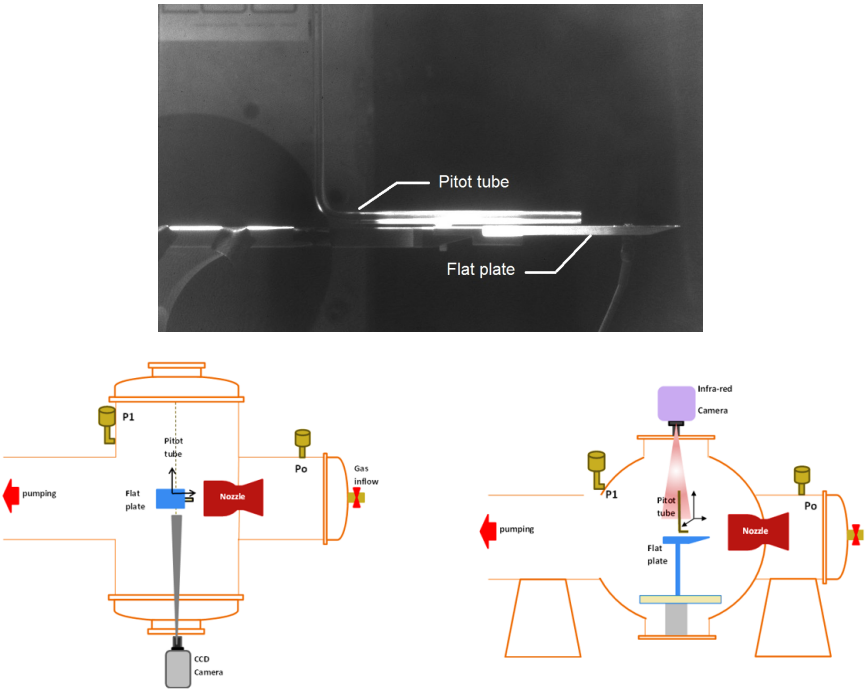

Figure 4 Figure 7 and Figure 8 of the Protocol part

Response to Reviewer 2

Manuscript Summary

The manuscript is definitely within the scope of the journal because it contains a complete test protocol and clear results. The paper could be published as-is.

Major Concerns

N/A

Minor Concerns

N/A

Manuscript Summary

N/A

Author's comment : We thank the Reviewer for its interest in our manuscript and her/his encouragements.

Response to Reviewer 3

Manuscript Summary

The draft manuscript proposes a new method for inducing drag in a Mach 4 rarefied flow (very high altitude–troposphere) as a way to soften a standard reentry. The method would use the ionization of the flow using a plasma actuator. In part, the manuscript is based on earlier work at Mach 2 [References 2 and 18] in which plasma effects become the dominant effect over thermal effects with an increase in the discharge current. In the present draft, it is recommended that Figure 5 and Figure 8 be shown side-by-side with the same flow direction along with a sketch showing the main effects. A juxtaposition as shown in Figure 7 of Reference 2 might also be considered in this regard. Although this reviewer is unfamiliar with the video concept behind this journal, I assume that the PROTOCOL's labeled A) thru G) are specifically written for this purpose. On page 7, I believe the actuator thickness should be 80 microns thick. With regard to the references, more care should be given to 2, 3, 10, and 21 to help the reader.

Major Concerns

N/A

Minor Concerns

N/A

Manuscript Summary

N/A

Author's comment : To make the fullest possible response, the Authors have listed the detailed comments given by the Reviewer and answered to each of the comment separately. We have also reproduced the previous and new versions, in order to highlight the modifications we made in agreement with the comments.

Reviewer comments

Reviewer's comment A: In the present draft, it is recommended that Figure 5 and Figure 8 be shown side-by-side with the same flow direction along with a sketch showing the main effects. A juxtaposition as shown in Figure 7 of Reference 2 might also be considered in this regard.

Answer A: We flip right to left the Figure 4 in order to get the same flow direction and we exchange the Figure 8 with another figure that shows the effect of the plasma actuator on the shock wave.

Therefore, we change these images:

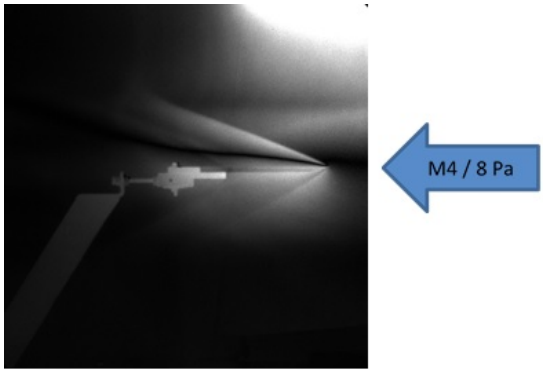

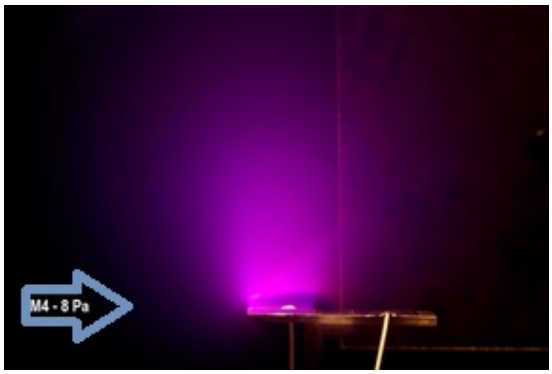

to these ones:

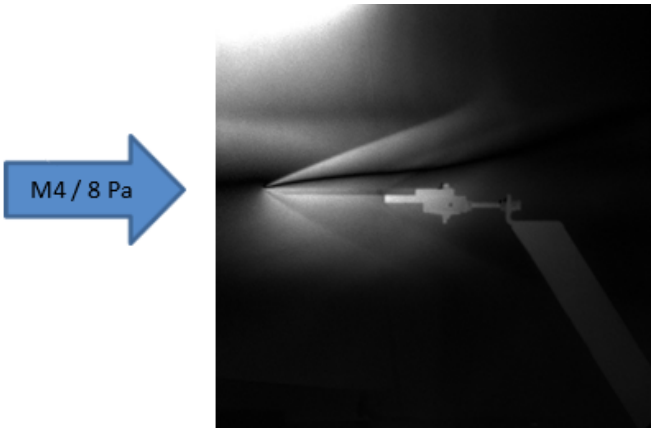

Reviewer's comment B: On page 7, I believe the actuator thickness should be 80 microns thick.

Answer B: Indeed, we did a mistaken on the units and thus, we correct it as follows:

L.345-346 The plasma actuator is composed of two aluminum electrodes, 50 mm-wide, 35 mm-long and 80 mm-thick.

to

L.345-346 The two electrodes setting the plasma actuator are manufactured in aluminium and designed with the dimensions: 50 mm-width, 35 mm-length and 80 μm-thickness.

Reviewer's comment C: With regard to the references, more care should be given to 2, 3, 10, and 21 to help the reader.

Answer C: We thank the Reviewer for this remark. Indeed we tried also to find the references with the informations we gave in the References part and were not able to find them. Therefore, we modified the references noted by the Reviewer and added more informations that were available, as for instance, the DOI numbers.

Response to Reviewer 4

Manuscript Summary

The manuscript provide details of an experimental method to utilize plasma actuator to control the flow in order to increase the drag and decrease the reentry speed. Most of the details have been provided. More detailed information about the drag should be provided to validate this technique.

Major Concerns

The language should be polished. Some description is not clear enough, which has been pointed out in the following section of the comments. The rational of the drag increase should be explained carefully since the future reader may not be familiar with plasma actuator.

Minor Concerns

See the section: Reviewer comments where each of the comments of the reviewers are listed and answered separately.

Manuscript Summary

N/A

> **Author's comment :** To make the fullest possible response, the Authors have listed the detailed comments given by the Reviewer and answered to each of the comment separately. We have also reproduced the previous and new versions, in order to highlight the modifications we made in agreement with the comments.

Reviewer comments

Reviewer's comment A: Line 44, it should be "the mapping of the flow pressures around the model."

> **Answer A:** Indeed, we thank the Reviewer for catching the error.
>
> **L.44-45** (...) for the mapping or the flow pressures around the model.
>
> to
>
> **L.44-45** (...) for the mapping of the flow pressures around the model.

Reviewer's comment B: Line 55, the sentence "Aerodynamic effects..." is not clear.

> **Answer B:** In order to clarify this sentence, we modify it.
>
> **L.56-58** Aerodynamic effects become increasingly important as the altitude decreases, and usually become dominant at 40 km, a result of the exponential increase of the air density as distance to the ground decreases.

to

L.56-58 Aerodynamic forces, as the drag and the lift, become increasingly important as the altitude decreases and usually become dominant at 40 km. It is due to the exponential increase of the air density when getting closer to the ground.

Reviewer's comment C: Line 59, it should be "Controlling the drag force is a method of..."

Answer C: As it is more elegant, we change the sentence as advised by the Reviewer.

L.60-61 Controlling the drag force is a mean of directly influencing (...)

to

L.60-61 Controlling the drag force is a method of directly influencing (...)

Reviewer's comment D: Line 79, it should be "higher than that in our experimental conditions."

Answer D: Indeed, we thank the Reviewer for catching the error.

L.81-82 (...) the use of the Schlieren technique shows that their working pressure is much higher that in our experimental condition.

to

L. 81-82 (...) the use of the Schlieren technique shows that their working pressure is much higher than that in our experimental condition.

Reviewer's comment E: Line 83, it should be "they are essentially numerical"

Answer E: Indeed, we thank the Reviewer for catching the error.

L.86-87 Other works are available but there are essentially numerical.

to

L.86-87 Other works are available but they are essentially numerical.

Reviewer's comment F: Line 90, it should be "Hence, the present work provides complementary databases and knowledge to other researchers working at higher pressure and thus higher Reynolds numbers"

Answer F: It turns out that some words of the sentence are missing and thus, the sentence is modified as advised by the Reviewer.

L.93-94 Hence, to bring complementary databases and knowledge with respect to other authors working at higher pressures and thus higher Reynolds number.

to

L.93-94 Hence, the present work provides complementary databases and knowledge to other researchers working at higher pressure and thus, higher Reynolds.

Reviewer's comment G: Line 120, it will be great if the author could provide a schematic of the electrode geometry indicating the radius of curvature of the rounded corner.

Answer G: We add the figure with the additional informations asked by the Reviewer. It is the Figure 2. Moreover, these required informations are added to the Protocol.

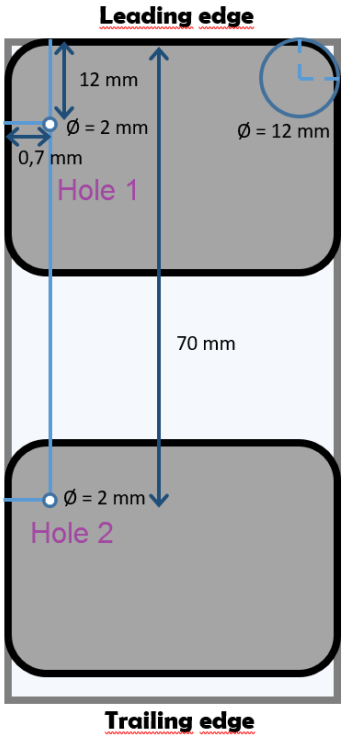

Reviewer's comment H: Line 131, it should be "trailing/leading edge angle"

Answer H: In order to five the missing information, we add it to the sentence.

p.5, L.55 Design the model (in this study, the model is beveled flat plate of 10cm-length, 5cm-width, 4mm-thickness and 15° angle).

to

p.5, L.55 Design the model (in this study, the model is beveled flat plate of 10cm-length, 5cm-width, 4mm-thickness and 15° leading edge angle).

Reviewer's comment I: Line 134 and 139, it will be more clear if the author could provide a figure showing the top view of the plate, in this figure, the dimension of the electrode and the location of the holes can be presented.

Answer I: We added the holes positions on the Figure 2. This figure has been included previously in this letter for the Comment G.

Reviewer's comment J: Line 142, it should be "This will help create roughness..."

Answer J: We thank the Reviewer for noting this grammar mistake.

L.147-148 This will help to create roughness and improve the electrode laying. In this case, the model is a beveled flat plate made in quartz.

to

L.147-148 This will help create roughness and improve the electrode laying. In this case, the model is a beveled flat plate made in quartz.

Reviewer's comment K: Line 150, "Moreover, choose glue with dilatation coefficient between those of quartz and aluminium to reduce tensions"

Answer K: The formulation given by the Reviewer is more elegant and thus, we modify the sentence.

L.155-157 Moreover chose a glue, which dilatation coefficient stands between those of the quartz and the aluminium to reduce tensions.

to

L.155-157 Moreover choose glue with dilatation coefficient between those of quartz and aluminium to reduce tensions.

Reviewer's comment L: Line 153, "Place the active electrode close to the leading edge and press it firmly to expel air bubbles. Indeed, if the air bubbles remain, they will inflate when the static pressure decreases and this will lead to detachment of the electrode."

Answer L: Again, the formulation given by the Reviewer is more elegant and thus, we modify the sentence.

L.157-159 Apply the active electrode close to the leading edge and press firmly to expel air bubbles. Indeed, if some air bubbles remain, they will inflate when lowering the pressure in the static pressure and this will lead to the detachment of the electrode.

to

L.157-159 Place the active electrode close to the leading edge and press it firmly to expel air bubbles. Indeed, if the air bubbles remain, they will inflate when the static pressure decreases and this will lead to detachment of the electrode.

Reviewer's comment M: Line 158, "Flip the flat plate over and add something heavy on top of it. This will flatten the electrodes against the flat plate."

Answer M: Again, the formulation given by the Reviewer is more elegant and thus, we modify the sentence.

L.162-163 Turn the flat plate and put on it something heavy. It will flatten the electrodes against the flat plate.

to

L.162-163 Flip the flat plate over and add something heavy on top of it. This will flatten the electrodes against the flat plate.

Reviewer's comment N: Line 162, "Use black paint, which can withstand high temperature, to draw a line along the central axis of the flat plate and two perpendicular lines passing through the center of each electrode"

Answer N: Again, the formulation given by the Reviewer is more elegant and thus, we modify the sentence.

L.166-168 Draw a line following the central axis of the flat plate and two perpendicular lines passing through the center of each electrode. Use for this a black paint withstanding high temperatures.

to

L.166-168 Use black paint, which can withstand high temperature, to draw a line along the central axis of the flat plate and two perpendicular lines passing through the center of each electrode.

Reviewer's comment O: Line 175, "Set the appropriate angle of attack with the adjustment wheel. If you give an angle of attack to the flat plate adjust the height of the standing pole because the back of the flat plate must coincide with the central axis of the flow." What does this mean?

Answer O: If you angle the model, it will no more be lined up with the nozzle axis. In order, to keep some work coherence, we chose the back of the flat plate as reference point. Therefore, the standing pole height must be adjusted to make the back of the flat plate and the nozzle axis coincide. The figure below can help to get the point. However, to make clearer this part, we modify it.

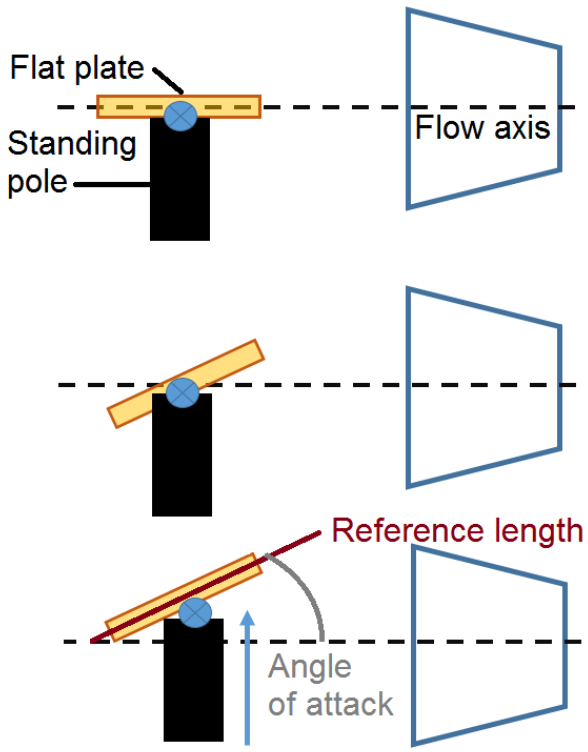

L.179-181 Set the appropriate angle of attack with the adjustment wheel. If you give an angle of attack to the flat plate, adjust the height of the standing pole because the back of the flat plate must coincide with the central axis of the flow. Check that the model fits in the core of the flow.

to

L.179-181 Set the appropriate angle of attack, defined as the angle between the flow axis and the model reference length (longitudinal model axis), with an angle gauge. Therefore, the trailing edge of the model would always coincide with the flow axis. Check that the model remains in the core of the flow (see Figure 6).

Reviewer's comment P: Line 178, How to determine if the model locates in the uniform core of the jet? Probably use Pitot probe or hot-wire to determine the velocity profile?

Answer P: The flow cores have been measured in the past with Pitot profiles and before using a nozzle we have never used before, we do again some Pitot measurements and establish the profiles in the three dimensional axis without model in order to confirm the flow core size.

Reviewer's comment Q: Line 179, please provide the detailed location of the thermocouple.

Answer Q: The thermocouple is used to measure the test chamber temperature so it can be located everywhere in the test chamber, excepted in the flow. Usually, we place it opposite to the model, 30 cm from it, to make sure that it does not interfere with the flow.

L.183-184 Set a 1mm wire-diameter K-type thermocouple in the test chamber to get the static temperature.

to

L.183-184 Set a 1mm wire-diameter K-type thermocouple to get the static temperature. Place it in the test chamber opposite to the model, at least 30 cm from the model in order to avoid interactions with the flow.

Reviewer's comment R: Line 198, is there any reference which indicates how to determine the diameter of the Pitot probe?

Answer R: We add the references we use to determine the ideal Pitot diameter. Especially the paper of Potter *et al.* (1990) which allows the determination of the orifice coefficients in order to get a reasonable effect. Taking into account the orifice coefficient, we will choose a Pitot diameter as big as possible in order to keep the measurement time small enough.

- S.A Schaaf : The Pitot probe in low-density flow. AGARD, Report 525, 1966.
- J. Potter et al. : An influence of the orifice on measured pressures in rarefied flow. AEDC-TDR, 64-175, 1964.
- J. Potter et al. : Techniques Expérimentales Liées à l'Aérodynamique à Basse Densité. AGARD, Report 318 (Fr), 1990.

Reviewer's comment S: Line 210, Calibrate the Labview program meant? What does this mean?

Answer S: The word "initialize" may be more appropriate. Indeed, we have a Labview program that helps us to acquire the Pitot measurements, drive the 3-axis robot. So, before each experiment, we open the program and enter the recording parameters.

L.215 Calibrate the Labview program meant for data acquisitions for this new test session.

to

L.215 Initialize the Labview program meant for data acquisitions for this new test session.

Reviewer's comment T: It will be better to provide a schematic of the Pitot probe to show the structure and design.

Answer T: We added an iCCD image of the Pitot tube above the flat plate in order to help visualizing its structure. The figure is noted as the Figure 7 in the manuscript and is introduced with this sentence.

L.364-366 (...)(see Figure 7 that shows the Pitot tube above the flat plate at position X = 50 mm, Y = 0 mm, Z = 0 mm which, corresponds to the middle of the flat plate)

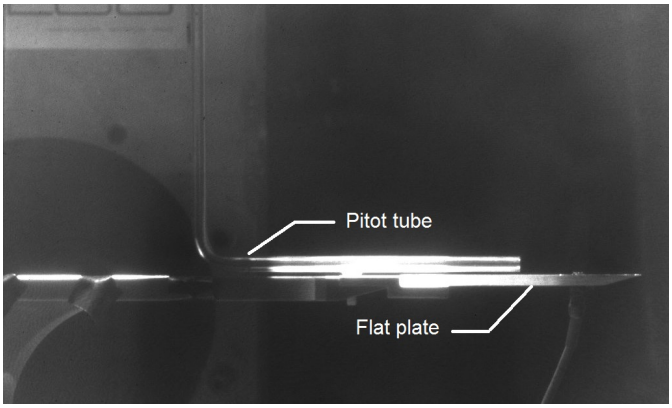

Reviewer's comment U: Line 226, How to estimate the emissivity of the painted electrode.

Answer U: We gave the method in the manuscript but it was not complete, therefore, we modify the part dedicated to the paint emissivity.

L.231-233 3.3 Estimate the emissivity of the painted electrode ε by measuring the surface temperature simultaneously with both the IR camera and a K-type thermocouple flush mounted on the flat plate surface.

to

L.231-233 3.3 Measure the surface temperature simultaneously with both the IR camera and a K-type thermocouple flush mounted on the flat plate surface. The temperature measured by the IR camera may differ from the one measured by the thermocouple as the initial calibration of the camera sets the emissivity ε at 1. If so, estimate the real emissivity of the black paint, as the ratio of the temperature given by the thermocouple on the temperature given by the IR camera.
3.4 Apply the real emissivity to the IR camera calibration to obtain the real surface temperatures with this device.
3.5 Set the good sensibility range of the camera according to the expected results during the test.

Reviewer's comment V: Line 390, any explanation on the difference between the experimental data and the numerical simulation?

Answer V: The boundary layer shape is not well reproduced by the simulation which suggests that for the DISIRAF code has to be improved in order to reproduce in a better way the shock wave for high Mach numbers. However, the z-position of the pressure peak is coherent with the numerical plot and this is precisely what was expecting when doing the simulations, in order to validate the experimental shock wave angles values.

Reviewer's comment W: Line 483 to Line 495, This paragraph should be the most important section of this article since the objective of the experiment discussed in present communication is to utilizing the plasma actuator to increase the drag and decrease the reentry speed of the vehicle. Some direct comparison of the drag and reentry

speed between the case with and without the plasma actuator should be presented in this section, using either table or figure. The drag should be determined by experimental method or estimated based on velocity or pressure data. The detail should be provided.

Answer W: Following your advice, we completely restructured the Discussion part with adding parts on the Protocol critical steps, the plasma actuators limitations and its future applications. We also enhanced the drag discussion and added two figures to illustrate the method for the drag estimation. One explains how we found an empirical law relating the shock wave angle and the drag coefficient and the other one presents the space shuttle re-entry guidance in terms of drag acceleration, as a function of the relative velocity, for the real trajectory and for the trajectory with an increase of 13 % for the drag coefficient. We hope that this new discussion answers your comments.

The temperature distributions with the infra-red camera measurements along the longitudinal axis of the plate are plotted on Figure 10. It is clear that the model surface is heated by the plasma actuator. Indeed, even if the heat source is strictly located at the cathode, the flat plate is entirely heated due to the quartz thermal conductivity. However, as the electric field varies along the X-direction, the longitudinal distribution of the surface temperature is not constant. The highest temperatures are measured close to the leading edge (i.e., above the cathode) where the electric field is the strongest and the lowest temperatures measured at the trailing edge of the flat plate. For a given value of IHV, the plasma discharge without the Mach 4 flow (static pressure set to 8 Pa) induced a similar heating of the flat plate (not shown here), since the temperature distribution is similar both in value and shape. This result confirms that heating of the flat plate surface is mainly related to a discharge effect and not influenced by the interaction between the Mach 4 air flow and the flat plate surface. The thermal equilibrium of the cathode temperature is reached after 1520 min; meaning that the magnitude order of the surface heating time scale is few tenth of minutes. It can be seen that the increase in surface temperature with the power discharge is not impactful. The same behavior was observed with the Mach 2 flow but with higher temperatures gradients. In rarefied flow regimes, one of the main effects expected to be responsible for the shock wave modification is the heating of the model surface. However, as it was demonstrated in previous studies, the surface heating accounted only for 50 % in the shock wave angle increase; thus, it can be assumed that the percentage would be even lower in the current case with the Mach 4 flow. Consequently the purely ionization effect is predominant in this case.

The surface heating induces a displacement effect: the flow viscosity above the heater is modified, inducing an increase in the laminar boundary layer thickness, and, consequently, the shock wave is shifted outward the flat plate surface (i.e., ? increases). This effect can be observed more clearly on Figure 11 where four Pitot pressure profiles are presented: one corresponds to the baseline, and the others correspond to the cases when different discharge powers are supplied. On the shape of the profiles measured at X = 50 mm, the knee geometry is found at a higher position on the Z-axis, meaning that the thickness of the boundary layer has increased and therefore, the shock wave angle too.

To demonstrate the efficiency of plasma actuators in the context of atmospheric entries, an estimation of the aerodynamic forces over the model has been made. The discussion is focused on the drag force because during atmospheric re-entries, it is directly linked with deceleration. In terms of relative variation, for a maximum wall temperature increase of almost 50%, the drag coefficient CD is modified by +13.0% for the plasma actuation. As the main goal is to decrease the speed of a spaceship, in view to decrease the total heat, it is interesting to study the effect of the drag diminution on the heat flux over the spaceship. For the re-entry of a space shuttle in the mold of Columbia, an increase of 13% of the total drag, as estimated in this paper, corresponds to a decrease in the vehicle speed of about 7% and of about 26% of the heat flow because the heat flow is proportional to the power 3.15 of speed. Taking into account that the mass of the heat protection in the shuttle is of 9575 kg and that the decrease of the heat flow is proportional to the mass protection, 2.5 tons of the Shuttle mass could be saved with the plasma actuator.

to

The described experimental protocol presents some critical steps. The first point concerns the repeatability of experiments because for a given experimental condition, several experimental campaigns are needed. Indeed, in order to have a complete physical analysis, different diagnostics are used that cannot be applied simultaneously. This implies that the experimental set-up (model, electrodes size and shape, position of the model in the test chamber, ?) must be rigorously the same throughout the experiments. Even slight differences can induce different discharges conditions modifying the plasma actuator effects and thus, the results will not anymore be comparable. The other point directly impacts the shock wave angle measurements. Indeed, each iCCD Image needs a specific post-processing, and thus, are analyzed manually. Therefore, it is essential to apply a well-run method for every post-processing. Furthermore, the shock wave angles are also determined from Pitot probe profiles and compared to angles detected with the iCCD images to strengthen the measurements.

The technique of plasma actuators itself presents also some issues. The main limitation of such actuators is due to the flow conditions, especially the pressure and thus, the altitude of the atmospheric re-entry spacecraft. Plasma actuators have to be characterized in different flow regimes in terms of speed and pressure to extrapolate their behavior in real cases. For this purpose, it is necessary to deeply understand the plasma physics and its coupling with the flow to overcome the challenges. Some authors incriminated thermal effects (bulk and surface) for the shock waves modifications in supersonic conditions. Shin et al. investigated thermal effects with two distinct discharge modes, where an increase in the gas temperature was observed nevertheless no clear evidence of plasma effects on the flow was identified.

The present paper shows that other physical aspects due to the discharge, than thermal ones, have to be taken into account to explain the flow modifications. Figure 16 displays the temperature distributions along the longitudinal axis of the model. The plots show that the plasma actuator heats the surface of the model although the distribution is non uniform and increases towards the cathode. The non-uniformity is induced by the variation of the electric field along the X-direction and this electric field is maximum close to the leading edge of the flat plate. For a given value of the discharge current IHV, the plasma discharge without the Mach 4 flow (static pressure set to 8 Pa) induced a similar heating of the flat plate, with a temperature distribution similar (both in value and shape) to the temperature distribution when the Mach 4 flow is operating. This result confirms that the heating of the flat plate surface is mainly related to a discharge effect and not influenced by the interaction between the Mach 4 air flow and the flat plate surface. Moreover, the surface heating induces a displacement effect: the flow viscosity above the heater is modified, inducing an increase in the laminar boundary layer thickness, and consequently, the shock wave is shifted outward the flat plate surface (i.e., the shock wave angle increases). This effect can be observed more clearly on Figure 17 where four Pitot pressure profiles are presented: one corresponds to the baseline, and the others correspond to the cases when different discharge powers are supplied. On the shape of the profiles measured at X = 50 mm, the knee geometry is found at a higher position on the Z-axis, meaning that the thickness of the boundary layer has increased and therefore, the shock wave angle too. Experiments carried out with a Mach 2 flow and a static pressure of 8 Pa, showed that the thermal effects accounted for only 50% in the shock wave angle increase and the remain 50% were due to ionization effects. For Mach 2 and Mach 4 flows, the surface temperature distributions are similar although the temperature gradients are higher with the Mach 2 flow. Therefore, one can assume that the ionization effect would be even greater with the Mach 4 flow than the 50 % estimated in previous studies, meaning that the influence of the surface heating on the shock wave modification will be even more negligible.

During atmospheric re-entries, atmospheric drag is used to slow down the vehicle, but the amount of energy to dissipate is enormous. The rate of energy dissipation is then estimated to be proportional to the cube of the vehicle speed, inducing very high temperatures on the spacecraft which may produce serious damages if the thermal protections are not sufficient. Optimal return trajectories are designed to obtain the minimum return cost defined as the sum of the mass propellant consumed by the space vehicle to de-orbit and the mass of thermal protections. However, reduction of thermal protections could be a way to decrease the cost of future missions. For this purpose, the idea is to increase the drag force in the aim of decelerating the vehicle and the use of plasma actuators could be an alternative method. In order to estimate the efficiency of plasma actuators in heat loads reduction, numerical simulations corresponding to our experimental conditions have been carried out to determine the aerodynamic drag forces induced by the discharge over the flat plate at Mach 2 and 8 Pa. The surface heating produced by the plasma discharge is numerically simulated reproducing the shock wave angle modifications observed experimentally. Results showed that the shock wave angles with only the surface heating are

Conclusions

The authors have applied a special care to answer to general remarks and questions of the reviewers. The Introduction section has been entirely modified, we added references in order to answer to the lack of information revealed by the reviewers. Other sections have been revised to agree with the reviewers comments. We hope that this revised version of our paper will satisfy attempts of the reviewers and the editor.

Finally, the authors thank the reviewers for their helpful reviewing and their constructive comments. It will be notified in acknowledgments as

... The authors would furthermore like to acknowledge the constructive feedback from the reviewers.

Yours sincerely,

The Authors